

**A novel porous graphitic carbon nitride ($\text{g-C}_7\text{N}_3$) substrate:
prediction of metal-based π -d conjugated nanosheets toward the
highly active and selective electrocatalytic nitrogen reduction
reaction**

Xian Wang, Qiang Zhang*, Weiju Hao, Chunyao Fang, Jianyang Zhou, and Jingcheng Xu

University of Shanghai for Science and Technology, Shanghai 200093, People's Republic of China

** Corresponding author.*

**Address correspondence to E-mail: qiangzhang@usst.edu.cn*

Note S1. Calculations of N₂ molecules adsorption energies

Adsorption energies (ΔE_{*N_2}) of N₂ molecules anchored on substrates by end-on and side-on patterns are determined by

$$\Delta E_{*N_2} = E_{*N_2} - E_* - E(N_2) \quad (1)$$

where E_{*N_2} , E_* and $E(N_2)$ denote the energies of N₂-TM@g-C₇N₃, the TM@g-C₇N₃ substrate and free N₂ molecules, respectively.

Note S2. Gibbs free energy calculations

The Gibbs free energy change (ΔG) for each elementary step was calculated based on the computational hydrogen electrode (CHE) model.¹ In this framework, the free energy of the electron-proton pair ($H^+ + e^-$) is half of the chemical potential of hydrogen based on the standard hydrogen electrode (SHE),² and the change of free energy was obtained by the following equation:

$$\Delta G = \Delta E + \Delta ZEP - T\Delta S + \Delta U + \Delta pH \quad (2)$$

where ΔE is the electronic energy difference of products and reactants in each elementary step and can be obtained from DFT calculation directly; ΔZEP and $T\Delta S$ are the change of zero-point energy correction and the entropy change at 298.15K, respectively. Calculated vibrational frequencies, zero-point energies and entropy of reaction intermediates are presented in Tables S5-S10. $\Delta U = -eU$, where e is the number of transferred electrons and U represents the applied electrode potential. $\Delta pH = k_B T \times pH \times \ln 10 = 0.059 pH$, where ΔpH included the pH effect and k_B is the Boltzmann constant.

Note S3. Theoretical faradaic efficiency

Hydrogen evolution reaction (HER) is a major competing reaction to NRR. Herein, to investigate the selectivity of NRR, we assume: (1) the catalytic selectivity based on theoretical Faradaic efficiencies can be estimated by the Boltzmann distribution,³ (2) Only HER and NRR are competing side reactions, (3) The proton and electron transfer are not the rate determining factors for both HER and NRR.

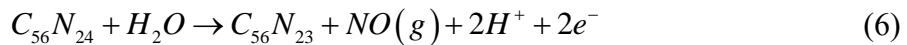
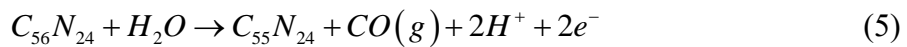
In this situation, the theoretical FE of NRR can be expressed as

$$FE = \frac{1}{1 + e^{-\frac{\delta G}{k_B T}}} \times 100\% \quad (3)$$

where δG is the Gibbs free energy difference of potential determination step between the HER and NRR, k_B represents the Boltzmann constant, and $T = 298.15$ K.⁴

Note S4. Electrochemical durability of the g-C₇N₃ support

The durability of materials is investigated because carbon/nitrogen atoms in g-C₇N₃ may decompose arising from their own nitrogen reduction reaction (NRR), carbon oxidation reaction (COR), and nitrogen oxidation reaction (NOR). During the real NRR process, it is thus crucial to evaluate the possibility of substrate decomposition. The process of degradation on g-C₇N₃ can be defined as follows:



Therefore, the free energy changes for NRR, COR and NOR can be written as

$$\Delta E_d = E_{C_{56}N_{23}} + E_{NH_3} - 3E_{(H^+ + e^-)} - E_{C_{56}N_{24}} \quad (7)$$

$$\Delta E_d = E_{C_{55}N_{24}} + E_{CO} + 2E_{(H^+ + e^-)} - E_{C_{56}N_{24}} - E_{H_2O} \quad (8)$$

$$\Delta E_d = E_{C_{56}N_{23}} + E_{NO} + 2E_{(H^+ + e^-)} - E_{C_{56}N_{24}} - E_{H_2O} \quad (9)$$

$$\Delta G_d = \Delta E_d + \Delta E_{ZPE} - T\Delta S \quad (10)$$

where $C_{56}N_{24}$, $C_{55}N_{24}$, $E_{C_{56}N_{23}}$, E_{NH_3} , $E_{(H^+ + e^-)}$, E_{CO} , E_{NO} and E_{H_2O} are the energies of g-C₇N₃ substrate, decomposed g-C₇N₃, NH₃, ($H^+ + e^-$) pair, CO, NO and H₂O, respectively. Therefore, the potential of electrochemical decomposition (U_d) can be given by

$$U_d = -\Delta G_d / ne \quad (11)$$

where n = 3 for NRR, while n = 2 for COR and NOR.⁵

Note S5. Diffusion energy barrier calculations

The diffusion energy barriers (G_{bar}) for the TM atom migration from the deposition site to the neighboring site are calculated by CI-NEB,⁶ the definition of the G_{bar} is defined as follow:

$$G_{bar} = G_{TS} - G_{IS} \quad (12)$$

where G_{IS} and G_{TS} represent the Gibbs free energies of the initial state and transition state, respectively. Taking W@g-C₇N₃ as a representative and its structures of initial (IS), transition (TS), and final (FS) state are plotted in Figure S23.

Table S1. The binding energy (E_b , in eV) of TM-atom anchored on g-C₇N₃, and charge transfer (Q, in e) of TM-atoms, corresponding to the most favorable configuration in energy. The “/” denotes that TM-atom move to other position after the structural optimization.

SACs	E_b (TM-N ₆)	E_b (TM-N ₂)	E_b (TM-N ₃)	Q (e)
Sc@g-C ₇ N ₃	/	-9.47	-9.46	1.73
Ti@g-C ₇ N ₃	/	-8.74	-8.73	1.48
V@g-C ₇ N ₃	/	-7.45	/	1.31
Cr@g-C ₇ N ₃	/	-6.02	-6.00	1.27
Mn@g-C ₇ N ₃	/	-5.88	-5.87	1.33
Fe@g-C ₇ N ₃	/	-5.82	-5.78	1.20
Co@g-C ₇ N ₃	/	-5.55	-5.53	0.89
Ni@g-C ₇ N ₃	/	-5.60	-5.49	0.81
Cu@g-C ₇ N ₃	/	-4.26	-4.21	0.81
Zn@g-C ₇ N ₃	/	-2.83	-2.75	1.14
Y@g-C ₇ N ₃	-8.82	/	/	2.14
Zr@g-C ₇ N ₃	/	-8.89	-8.89	1.89
Nb@g-C ₇ N ₃	/	-7.92	-7.92	1.62
Mo@g-C ₇ N ₃	/	-6.87	-6.87	1.28
Ru@g-C ₇ N ₃	/	-7.10	/	0.94
Rh@g-C ₇ N ₃	/	-6.18	/	0.68
Pd@g-C ₇ N ₃	/	-4.27	/	0.68
Ag@g-C ₇ N ₃	-3.74	/	/	0.65
Cd@g-C ₇ N ₃	/	-3.07	-3.07	1.18
Hf@g-C ₇ N ₃	/	-10.28	-10.28	1.72
Ta@g-C ₇ N ₃	/	-9.75	-9.76	1.64
W@g-C ₇ N ₃	/	-8.18	-8.19	1.39
Re@g-C ₇ N ₃	/	-7.59	-7.61	1.28
Os@g-C ₇ N ₃	/	-6.38	-6.60	0.82
Ir@g-C ₇ N ₃	/	-6.55	-6.56	0.71
Pt@g-C ₇ N ₃	/	-5.58	-5.58	0.69
Au@g-C ₇ N ₃	/	-3.02	-3.01	0.54

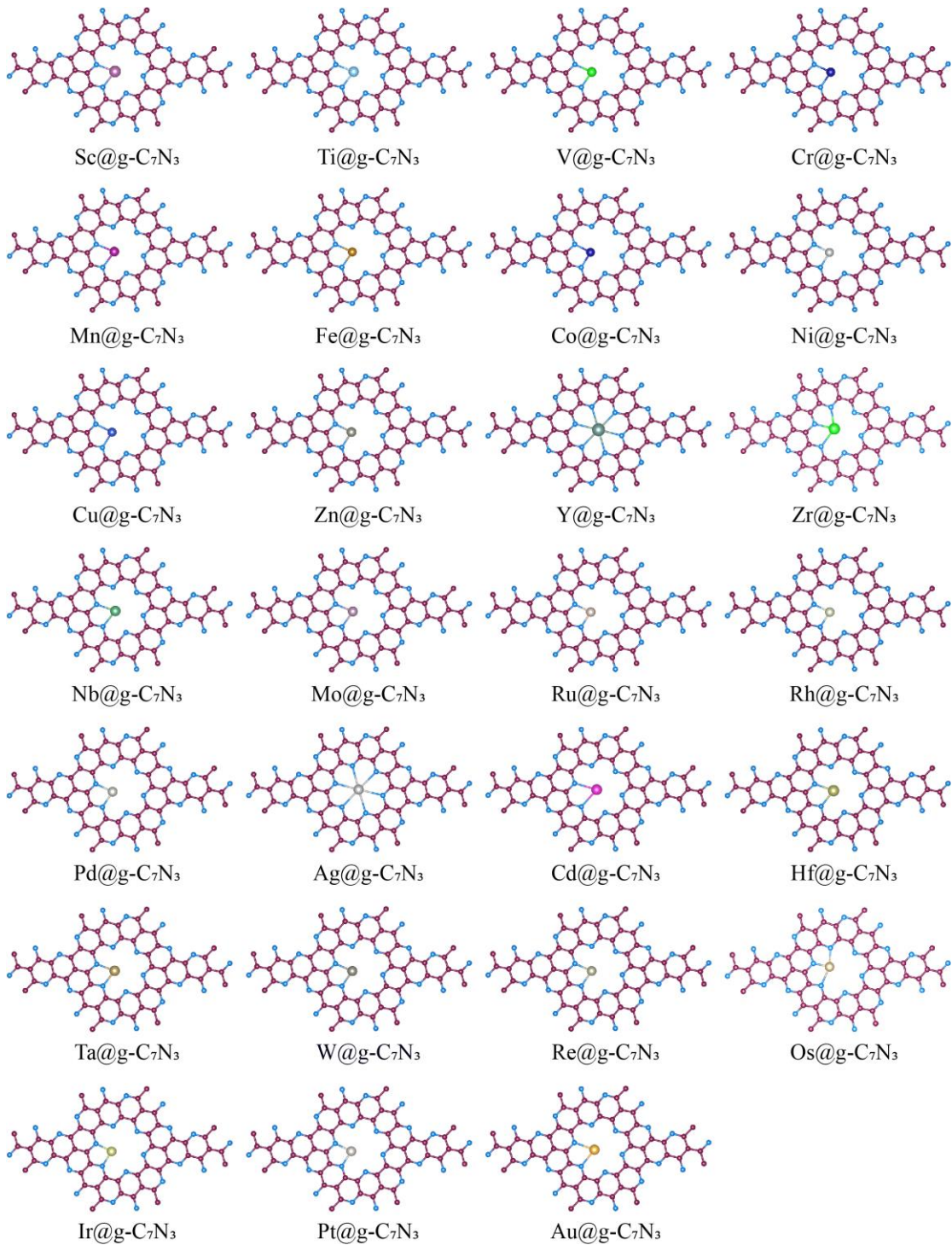


Figure S1. Well-optimized configurations of TM-atom anchored on $\text{g-C}_7\text{N}_3$.

Table S2. The adsorption energies (ΔE_{*N_2}) of the N₂ molecules anchored on the TM@g-C₇N₃ monolayer via two different patterns (end-on and side-on), the TM-N and the N-N bond lengths of each TM@g-C₇N₃ are also listed.

	end-on			side-on			
	ΔE_{*N_2} (eV)	TM-N (Å)	N-N (Å)	ΔE_{*N-N} (eV)	TM-N (Å)	TM-N (Å)	N-N (Å)
Sc	-0.33	2.22	1.122	0.08	2.46	2.36	1.138
Ti	-0.63	2.04	1.129	-0.03	2.24	2.24	1.149
V	-0.34	1.97	1.128	-0.34	1.97	3.10	1.128
Cr	0.04	2.16	1.118	0.06	2.16	3.25	1.119
Mn	-0.01	2.18	1.116	0.34	2.88	2.89	1.117
Fe	-0.27	1.95	1.125	0.23	2.20	2.20	1.139
Co	-0.46	1.86	1.125	0.16	2.14	2.06	1.143
Ni	-0.20	1.86	1.123	-0.20	1.86	2.97	1.123
Cu	-0.28	1.83	1.123	0.27	2.44	3.09	1.117
Zn	0.11	2.23	1.114	0.34	3.19	3.27	1.114
Y	-0.26	2.42	1.121	0.14	2.66	2.66	1.133
Zr	-0.94	2.15	1.134	-0.38	2.32	2.32	1.160
Nb	-0.53	1.99	1.142	0.08	2.14	2.15	1.185
Mo	-0.25	1.96	1.139	0.37	2.21	2.21	1.164
Ru	-0.54	1.86	1.137	-0.54	1.86	2.99	1.137
Rh	-0.20	1.96	1.126	0.30	2.66	3.49	1.118
Pd	0.12	2.02	1.121	0.31	3.02	3.72	1.115
Ag	0.30	2.78	1.114	0.32	3.34	3.60	1.114
Cd	0.20	2.66	1.113	0.31	3.15	3.64	1.114
Hf	-0.94	2.09	1.137	-0.38	2.24	2.24	1.173
Ta	-0.61	1.99	1.146	-0.03	2.09	2.09	1.205
W	-0.59	1.95	1.143	0.22	2.08	2.08	1.200
Re	-0.64	1.89	1.144	0.32	2.18	2.18	1.171
Os	-1.05	1.91	1.137	0.28	2.21	2.21	1.159
Ir	-0.53	1.94	1.129	0.33	3.18	3.83	1.115
Pt	0.33	3.37	1.114	0.31	3.56	4.09	1.114
Au	0.33	3.02	1.115	0.31	3.33	3.91	1.114

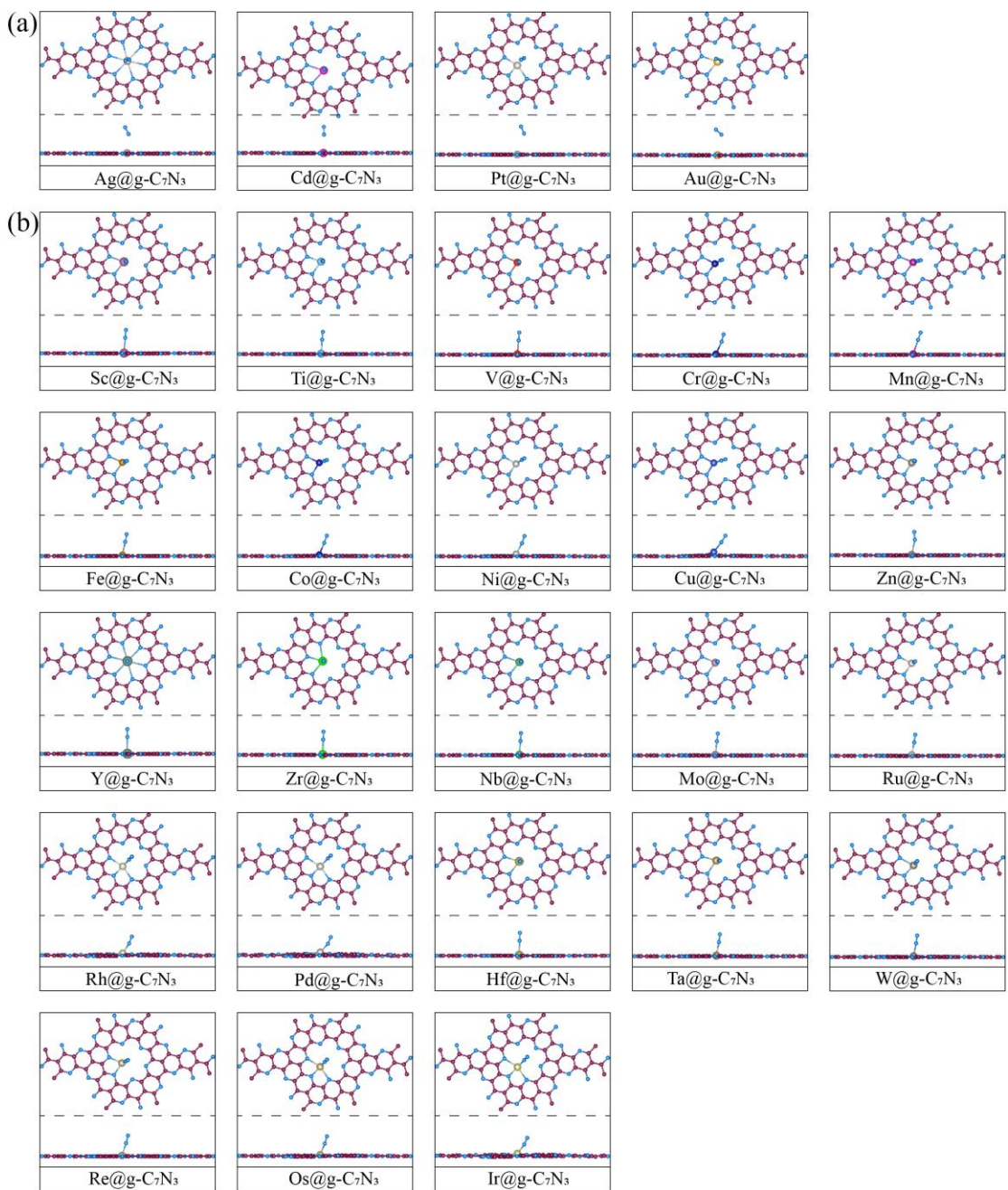


Figure S2. The well-optimized N₂ adsorption configurations on TM@g-C₇N₃ via end-on model, in which (a) and (b) are correspond to physisorption and chemisorption, respectively.

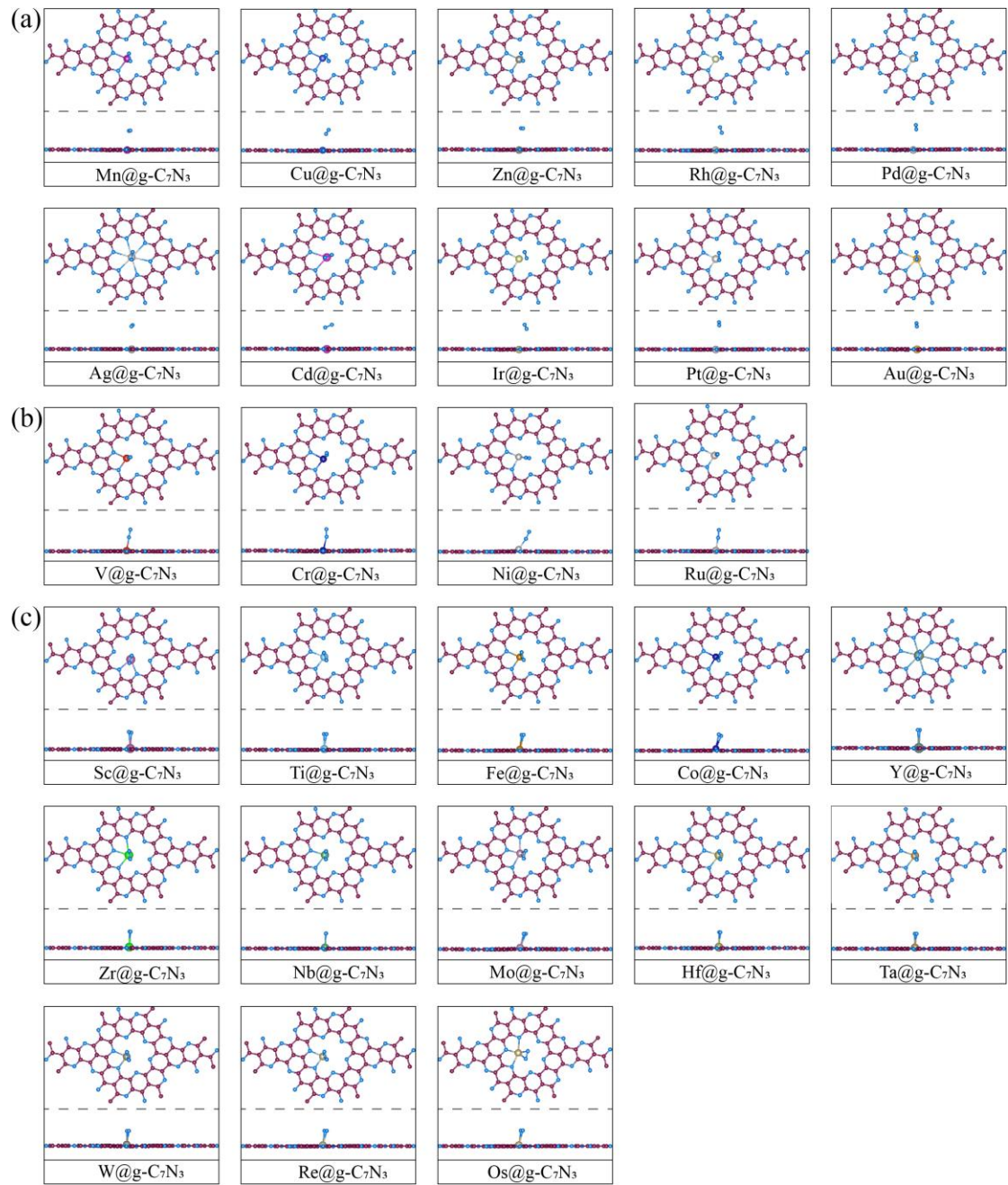


Figure S3. The well-optimized N₂ adsorption configurations on TM@g-C₇N₃ via side-on model: (a) represents physisorption; (b) and (c) correspond to chemisorption. After the structures are fully optimized, the four configurations in (b) are changed from side-on pattern to end-on pattern.

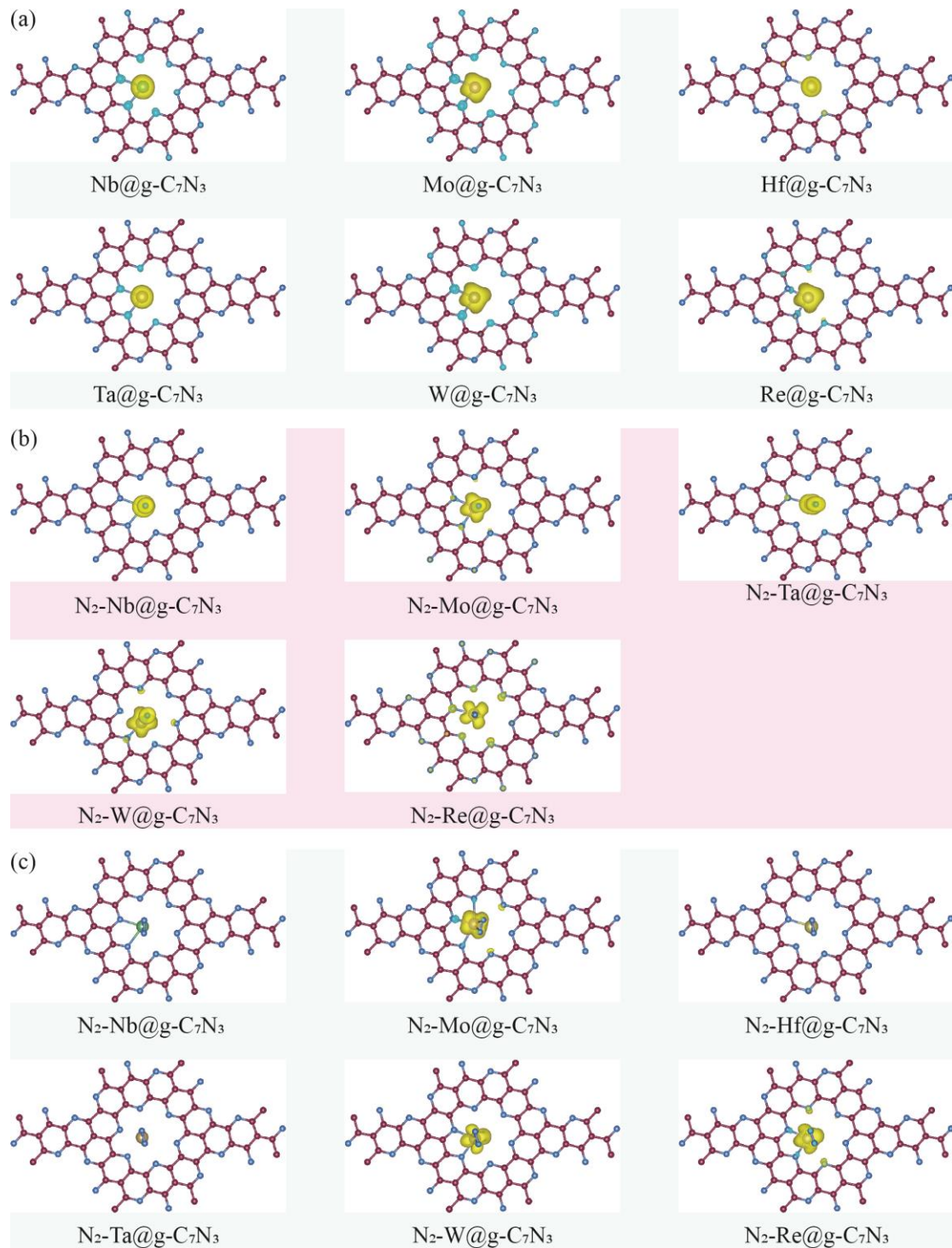


Figure S4. Spin-polarized charge density with the isosurface value of 0.03 e/Å³: (a) TM@g-C₇N₃; (b) N₂ adsorbed on TM@g-C₇N₃ with end-on pattern; (c) N₂ adsorbed on TM@g-C₇N₃ with side-on pattern. Here, TM represents Nb, Mo, Hf, Ta, W, and Re.

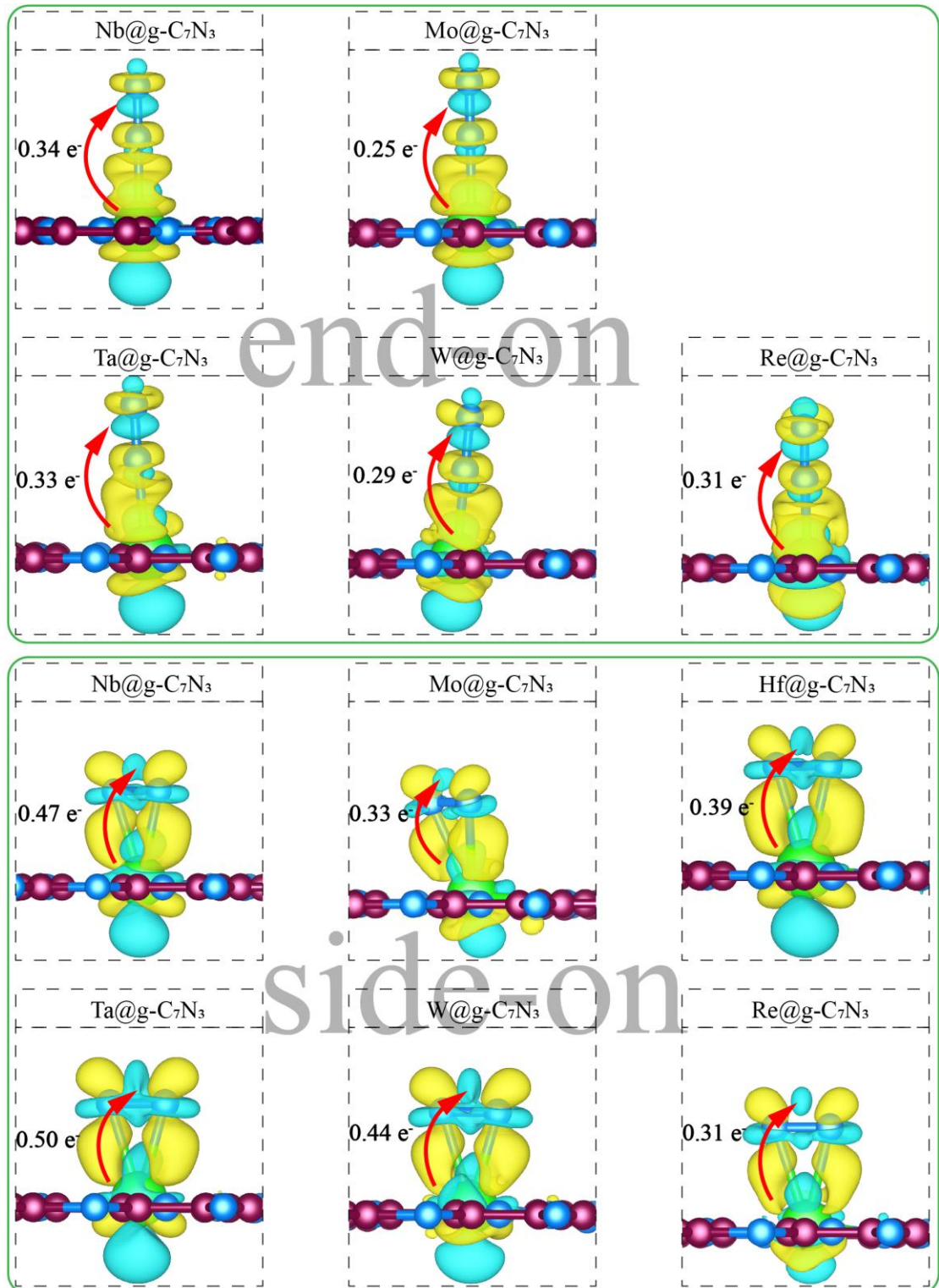


Figure S5. Difference charge density of Nb, Mo, Ta, W and Re@g-C₇N₃ with the adsorption of N₂ via end-on (up) and side-on (down) patterns as well as Hf@g-C₇N₃ with the adsorption of N₂ via side-on pattern. The isosurface value is 0.03 $e/\text{\AA}^3$.

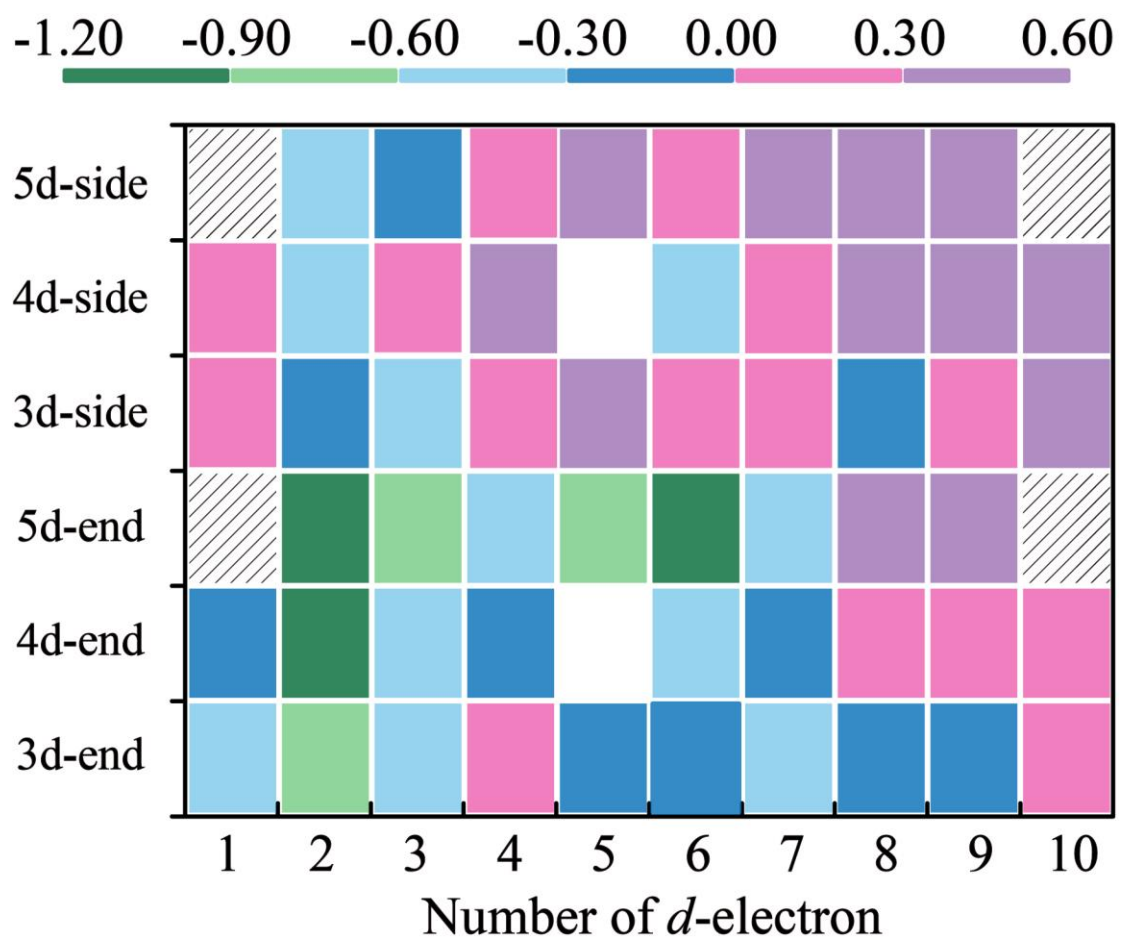


Figure S6. Relationship between the adsorption energy of N₂ (ΔE_{*N_2}) and the number of d-electrons.

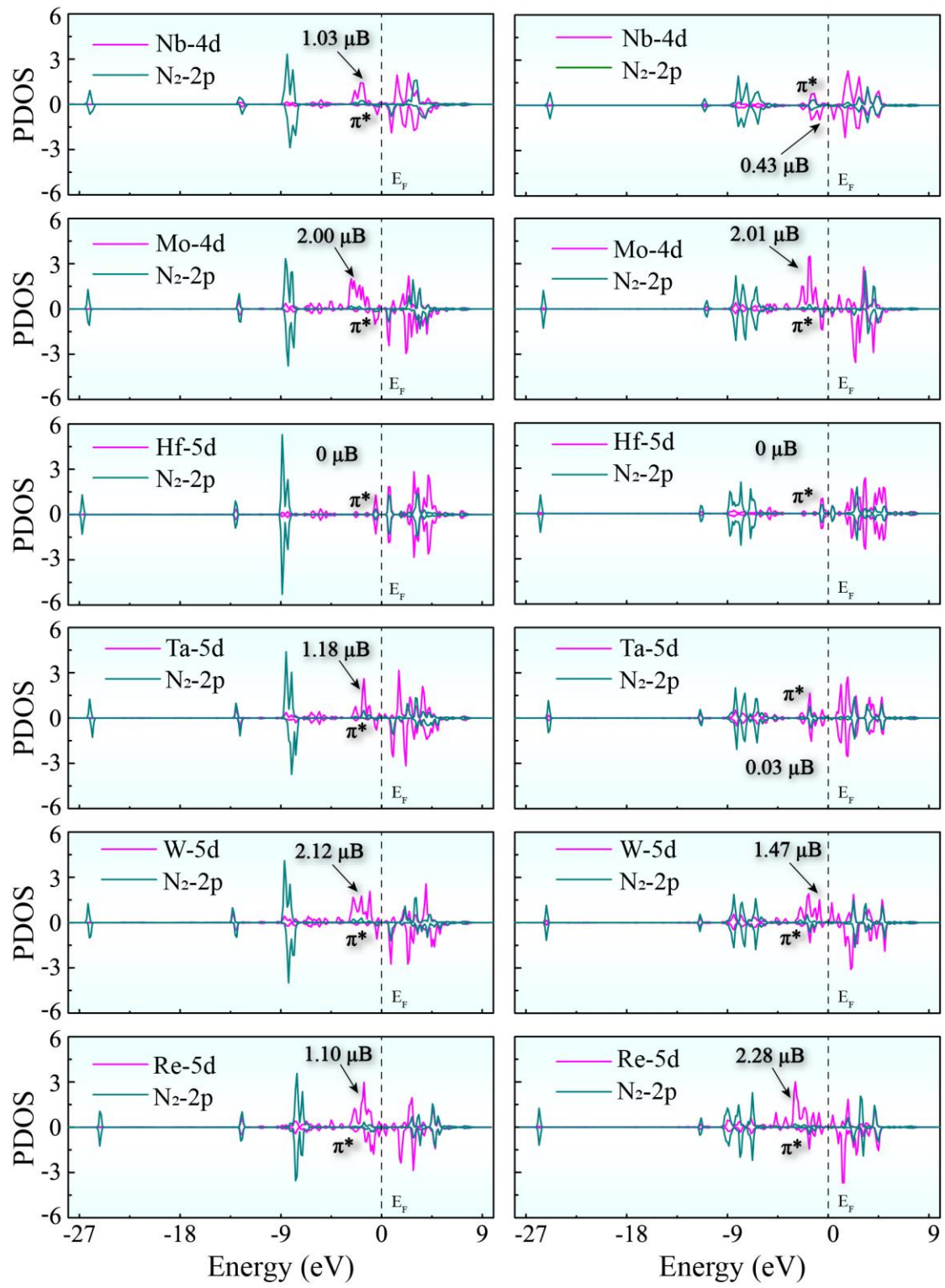


Figure S7. Projected density of states (PDOS) of Nb, Mo, Hf, Ta, W and Re as well as N₂ after the adsorption of N₂ via end-on (left) and side-on (right) patterns. The Fermi level is set to 0 eV.

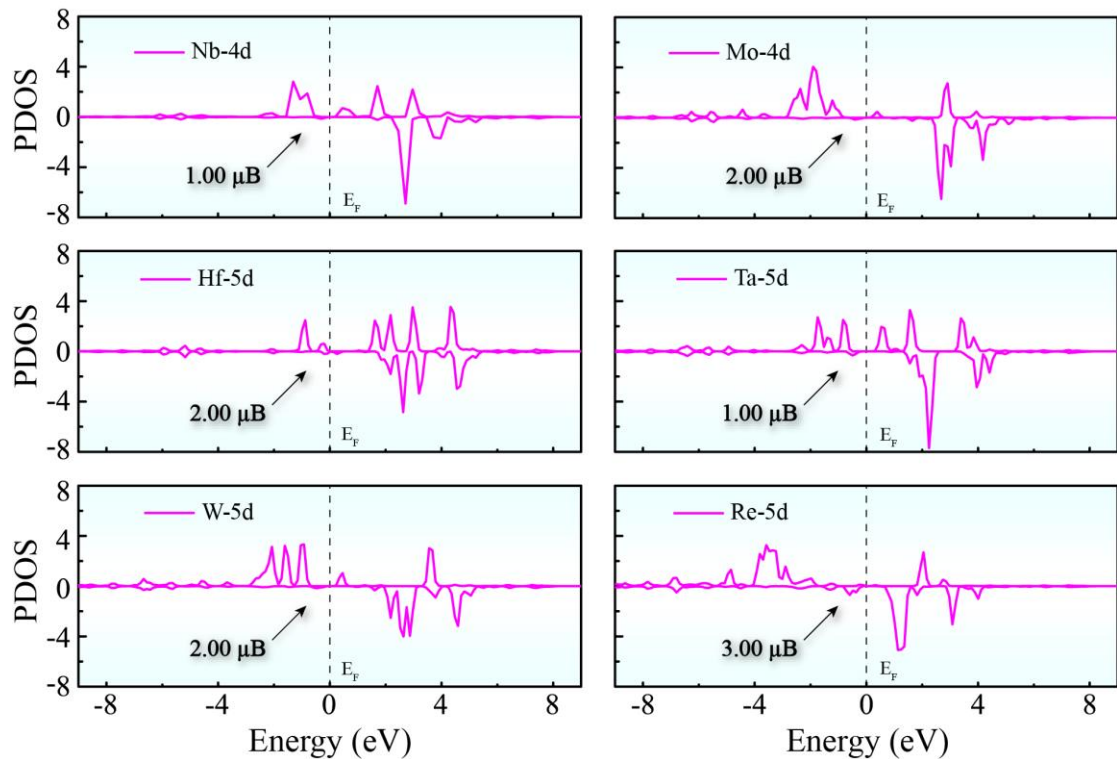


Figure S8. Projected density of states (PDOS) of Nb, Mo, Hf, Ta, W and Re@g-C₇N₃ before the adsorption of N₂. Fermi level is set to be 0 eV.

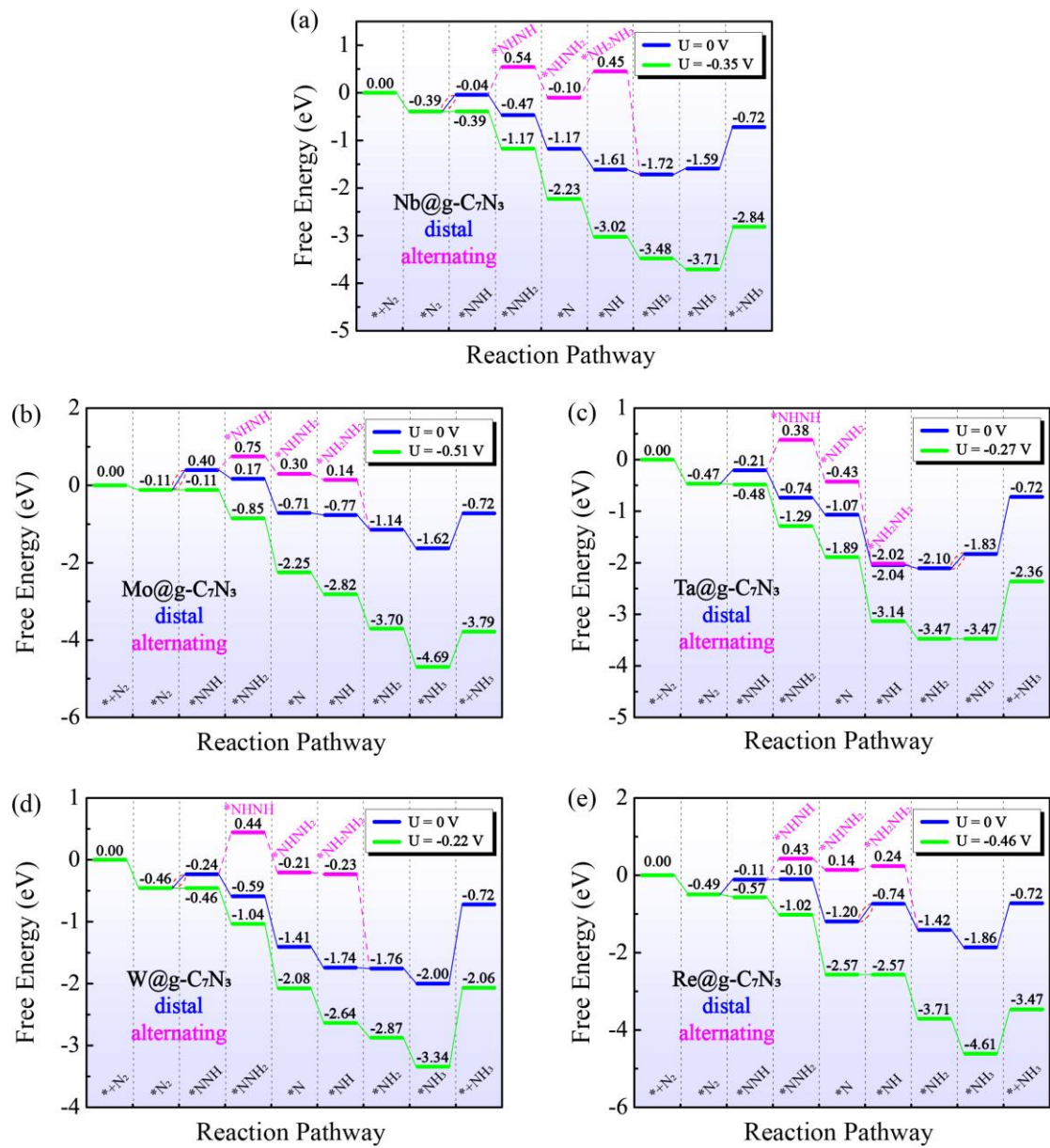


Figure S9. Free energy diagrams of NRR at different applied potentials on (a) Nb@g-C₇N₃, (b) Mo@g-C₇N₃, (c) Ta@g-C₇N₃, (d) W@g-C₇N₃, and (e) Re@g-C₇N₃ along distal pathway.

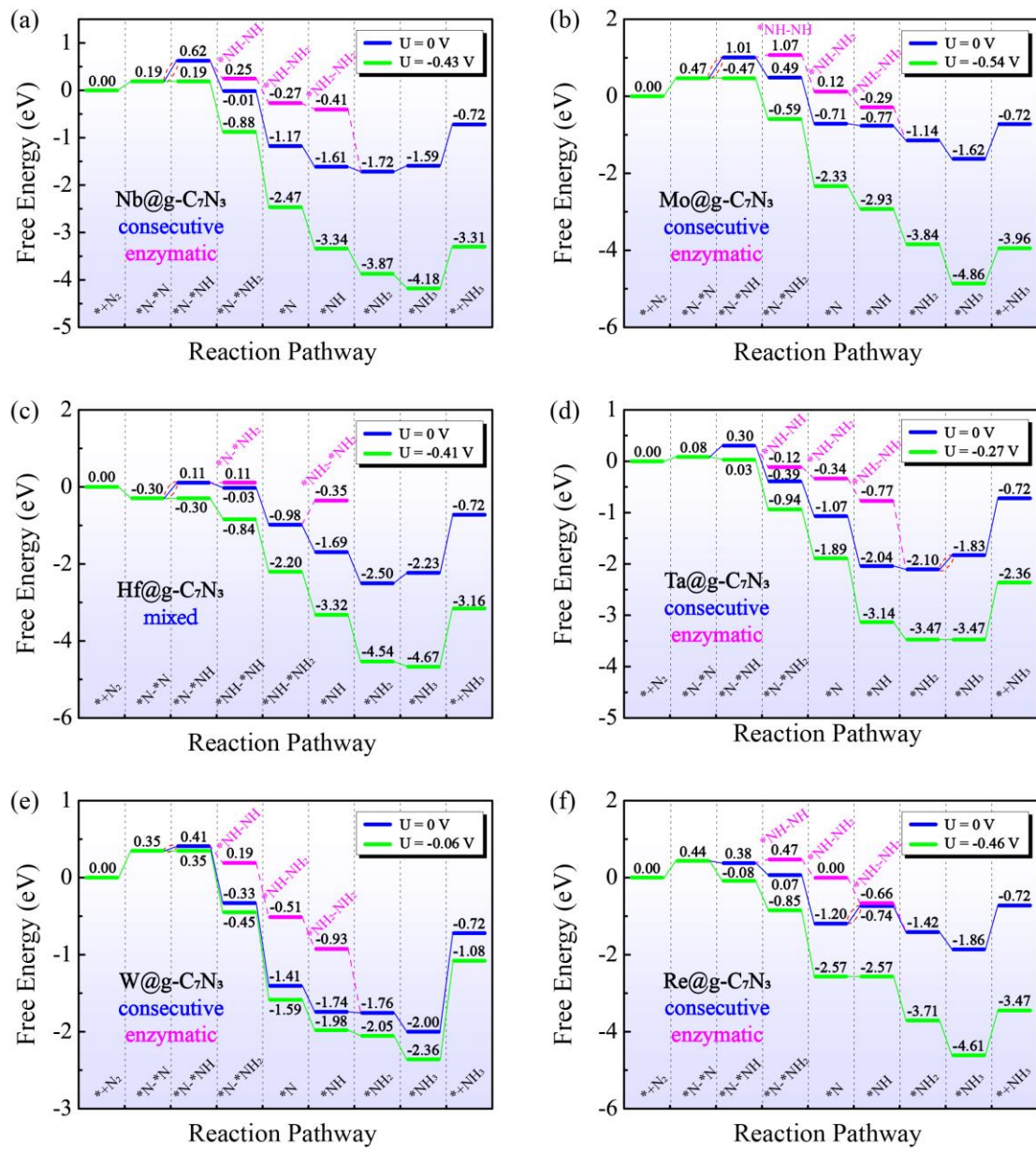


Figure S10. Free energy diagrams of NRR at different applied potentials on (a) Nb@g-C₇N₃, (b) Mo@g-C₇N₃, (c) Hf@g-C₇N₃, (d) Ta@g-C₇N₃, (e) W@g-C₇N₃, and (f) Re@g-C₇N₃. Except that Hf@g-C₇N₃ follows mixed pathways, the others follow consecutive pathways.

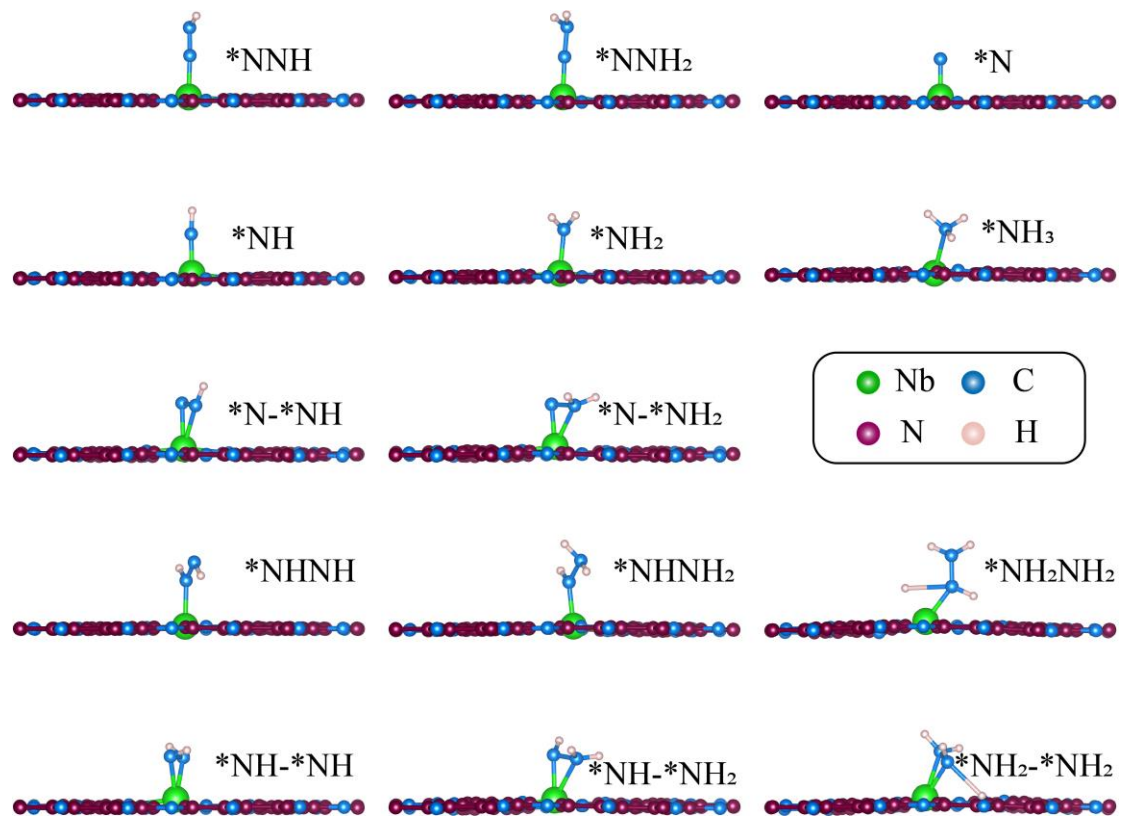


Figure S11. Well-optimized structures of reaction intermediates on Nb@g-C₇N₃ surface.

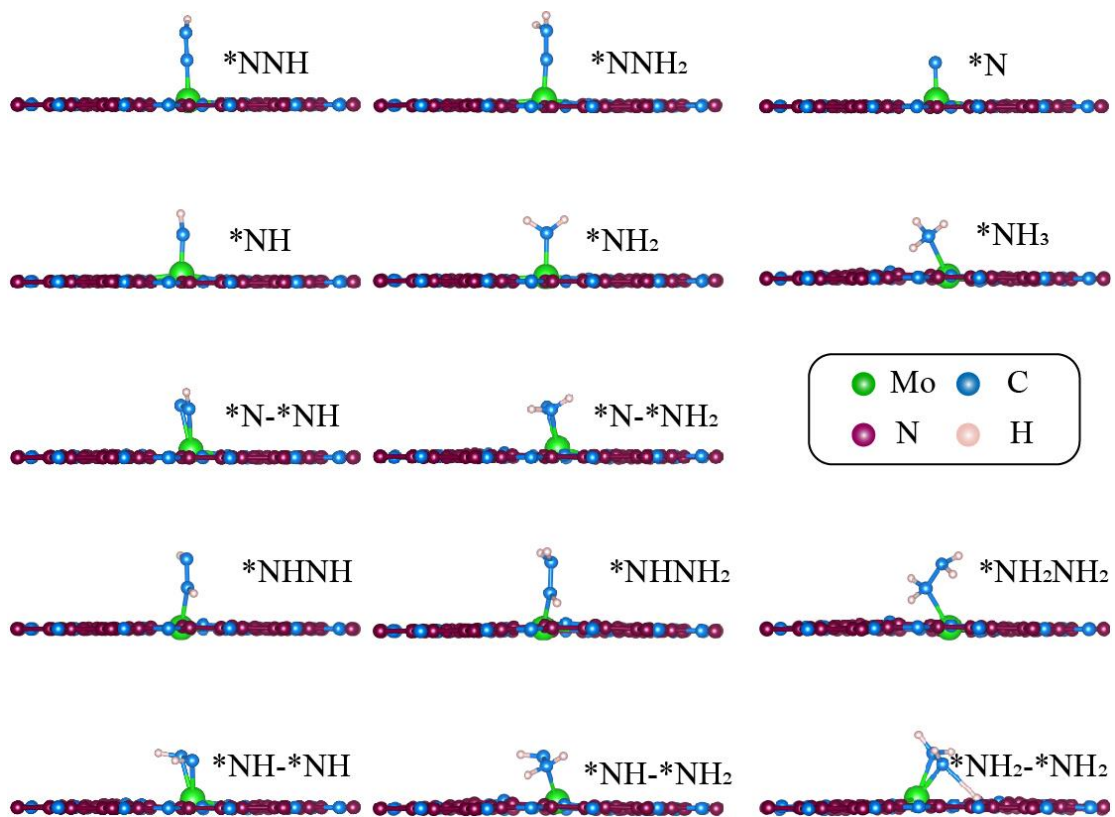


Figure S12. Well-optimized structures of reaction intermediates on $\text{Mo@g-C}_7\text{N}_3$ surface.

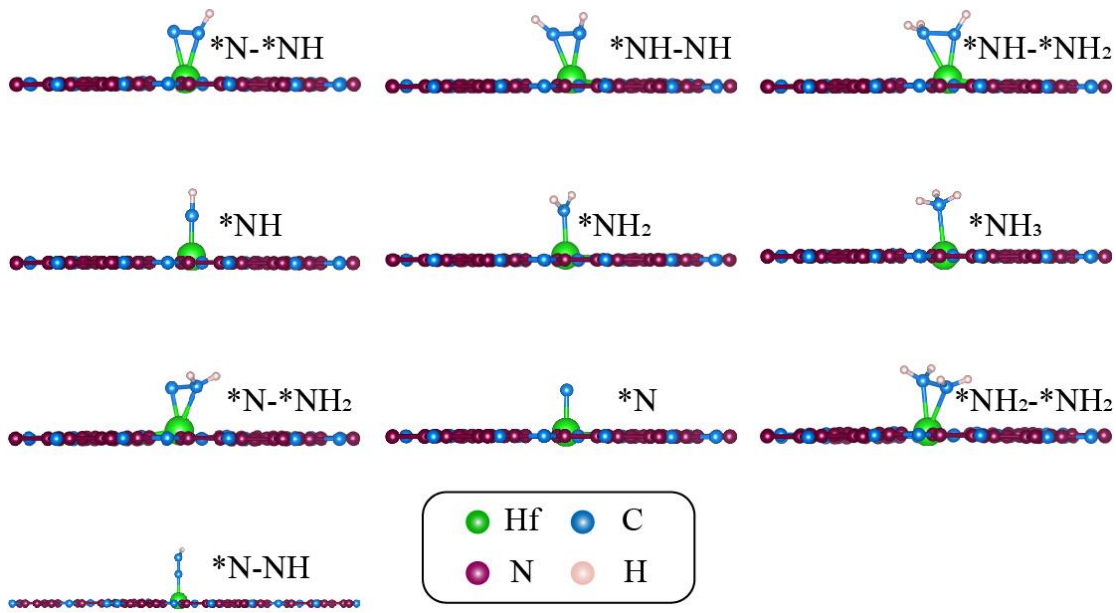


Figure S13. Well-optimized structures of reaction intermediates on Hf@g-C₇N₃ surface.

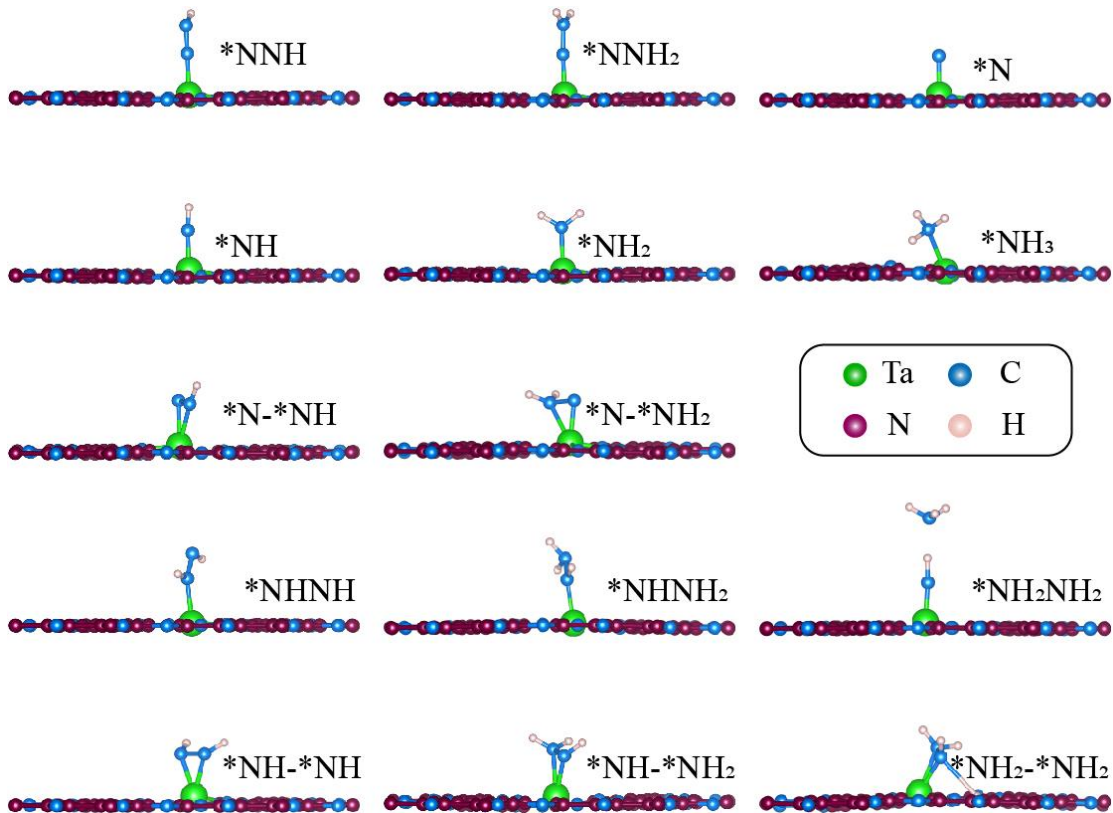


Figure S14. Well-optimized structures of reaction intermediates on Ta@g-C₇N₃ surface.

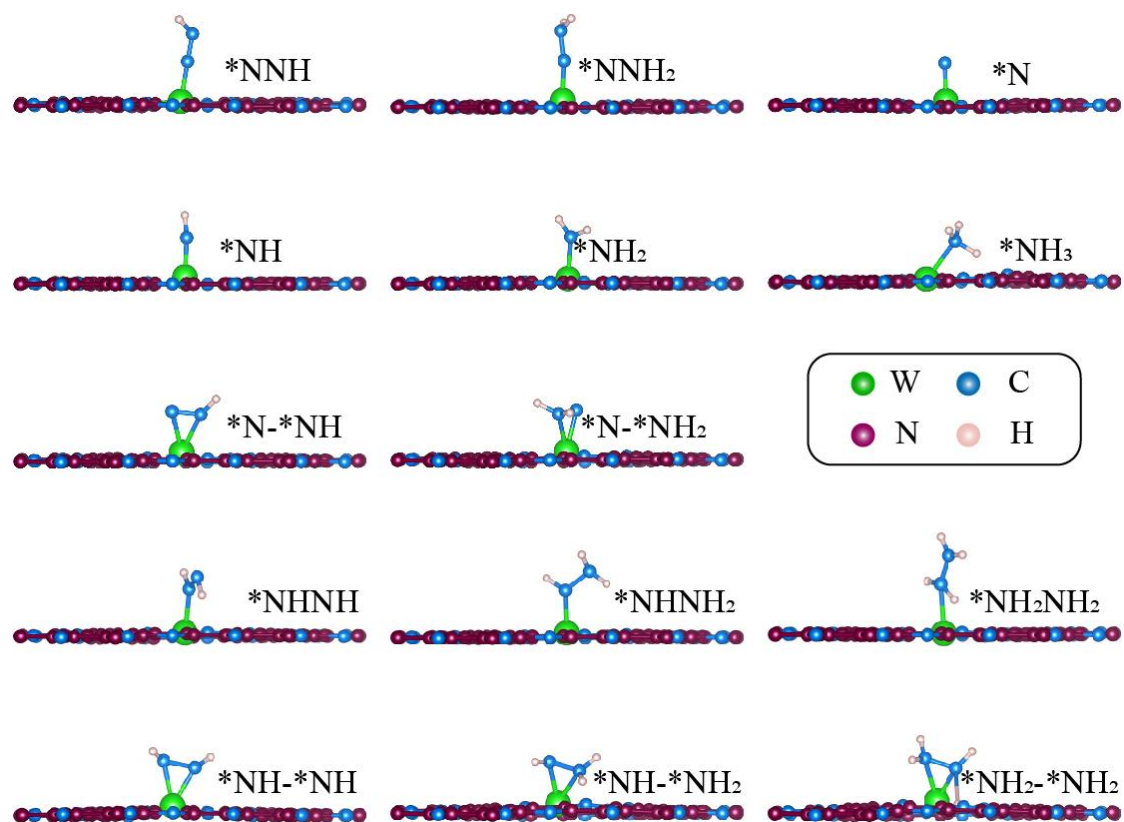


Figure S15. Well-optimized structures of reaction intermediates on W@g-C₃N₃ surface.

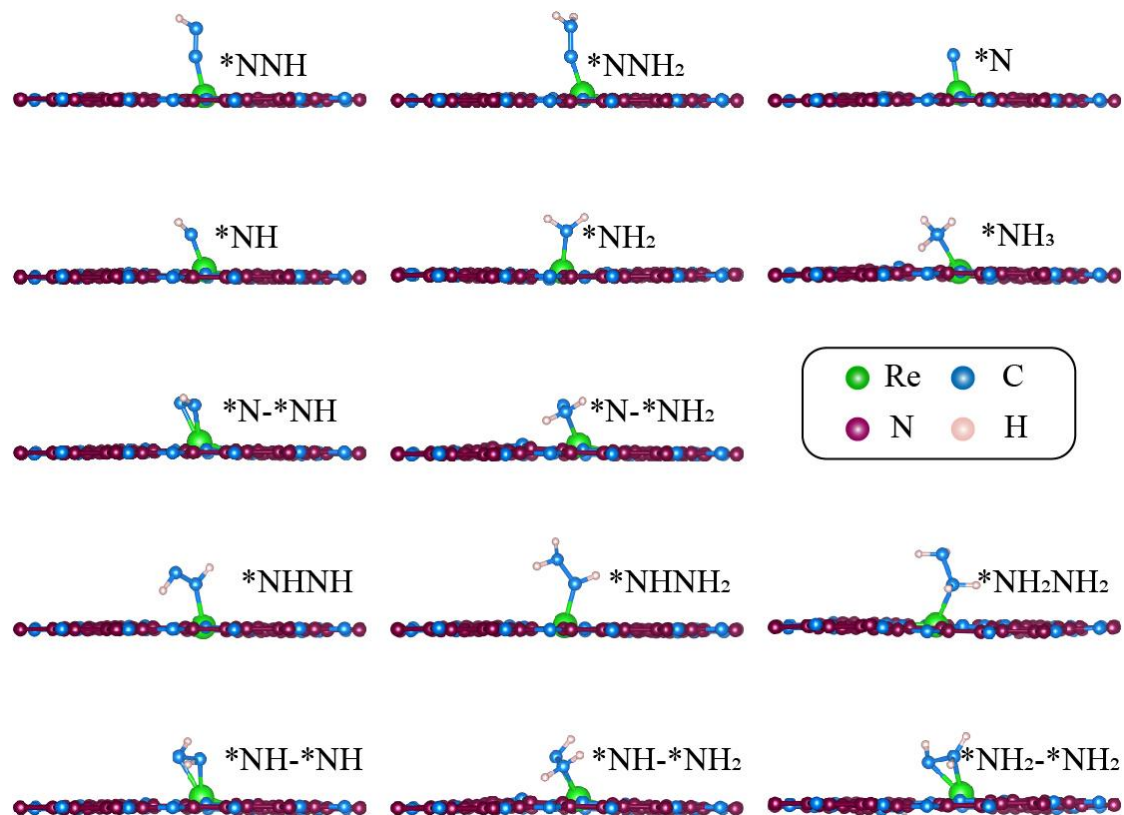


Figure S16. Well-optimized structures of reaction intermediates on Re@g-C₇N₃ surface.

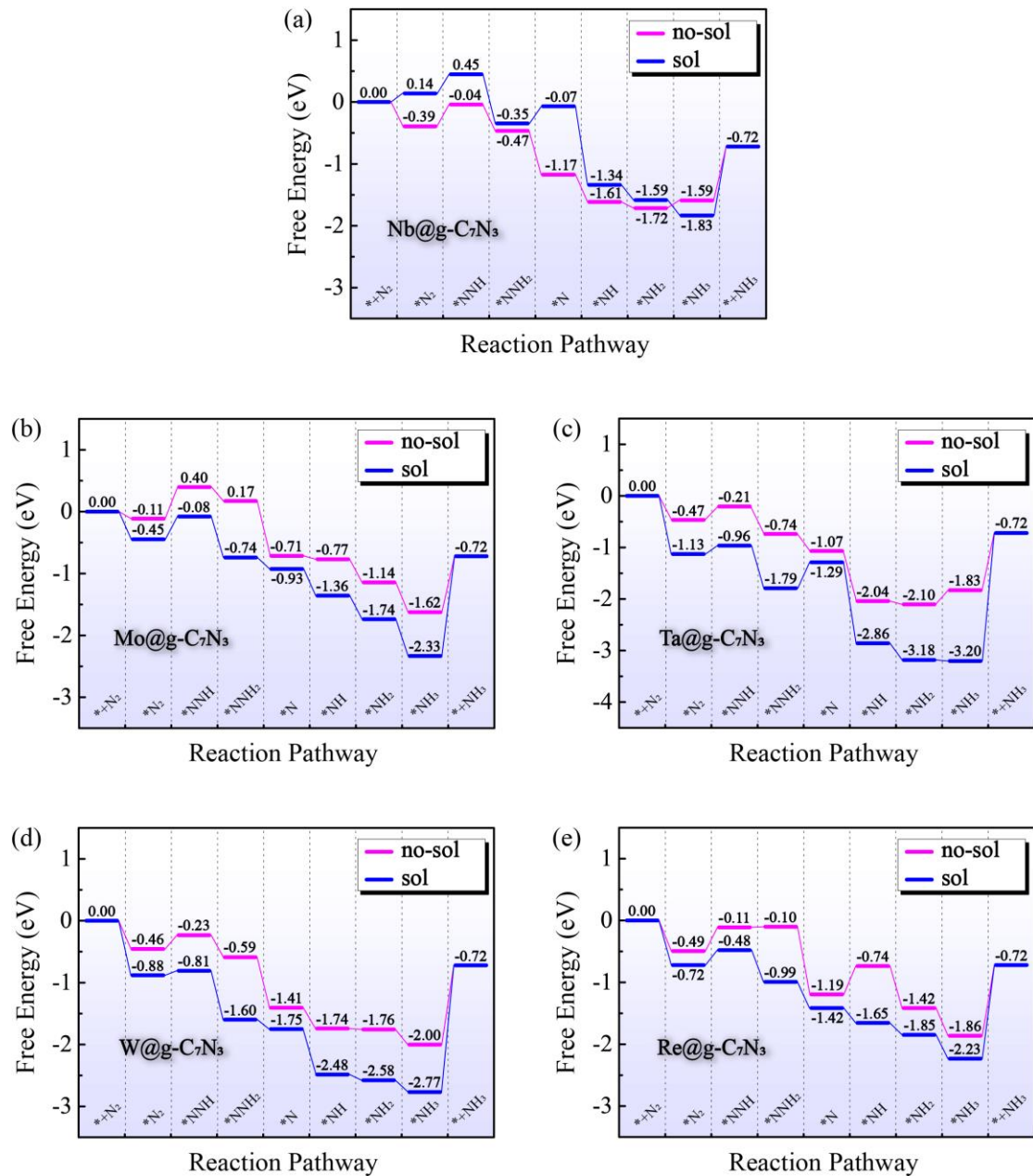


Figure S17. Free energy diagrams of NRR on Nb, Mo, Ta, W, and Re@g-C₇N₃ without/with solvent effect along the energetically favorable distal pathway. The applied potentials are set to 0 V.

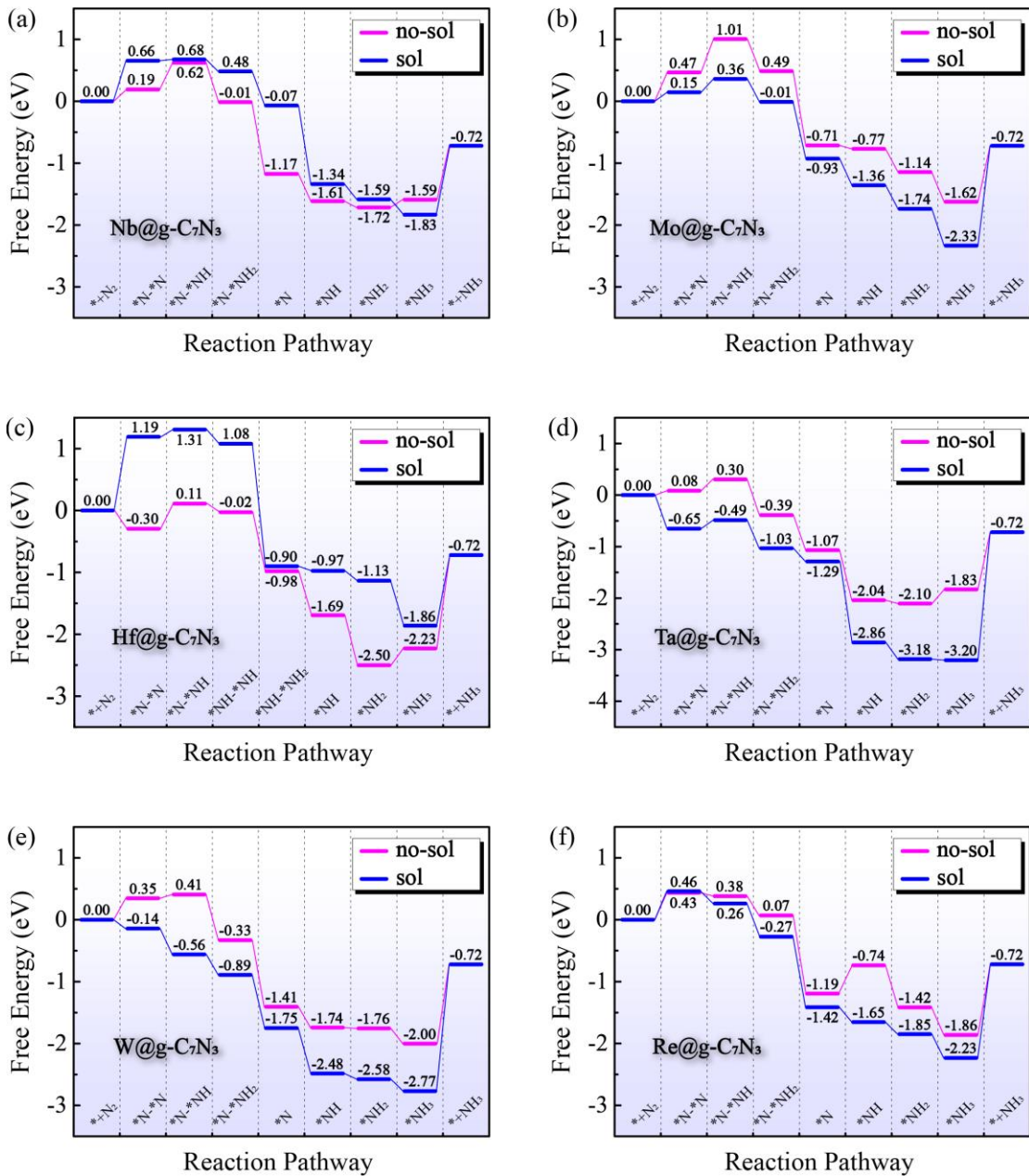


Figure S18. Free energy diagrams of NRR on Nb, Mo, Hf, Ta, W, and Re@g-C₇N₃ without/with solvent effect along the energetically favorable consecutive pathway, Hf@g-C₇N₃ along the energetically favorable mixed pathway. All applied potentials are set to 0 V.

Table S3. Limiting potentials (U_L) of NRR on Nb, Mo, Hf, Ta, W, and Re@g-C₇N₃ without/with solvent effect via end-on (left) and side-on (right) patterns.

TM	U_L (end-on)		U_L (side-on)	
	no-sol (V)	sol (V)	no-sol (V)	sol (V)
Nb	-0.35	-0.31	-0.43	-0.66
Mo	-0.51	-0.37	-0.54	-0.22
Hf	/	/	-0.41	-1.19
Ta	-0.27	-0.50	-0.27	-0.16
W	-0.22	-0.07	-0.06	0
Re	-0.46	-0.24	-0.46	-0.46

Table S4. Limiting potentials of NRR ($U_L(NRR)$) and HER ($U_L(HER)$) on Nb, Mo, Ta, W, and Re@g-C₇N₃ along distal/ consecutive pathway and Hf@g-C₇N₃ along mixed pathway. $\Delta U_{NRR-HER}$ denotes the limiting potentials difference between $U_L(NRR)$ and $U_L(HER)$.

end-on (V)			side-on (V)			
$U_L(HER)$	$U_L(NRR)$	$\Delta U_{NRR-HER}$	$U_L(HER)$	$U_L(NRR)$	$\Delta U_{NRR-HER}$	
Nb	-0.32	-0.35	-0.03	-0.32	-0.43	-0.11
Mo	-0.10	-0.51	-0.41	-0.10	-0.54	-0.44
Hf				-0.64	-0.41	0.24
Ta	-0.65	-0.27	0.37	-0.65	-0.27	0.37
W	-0.5	-0.223	0.28	-0.5	-0.35	0.15
Re	-0.60	-0.46	0.14	-0.60	-0.46	0.14

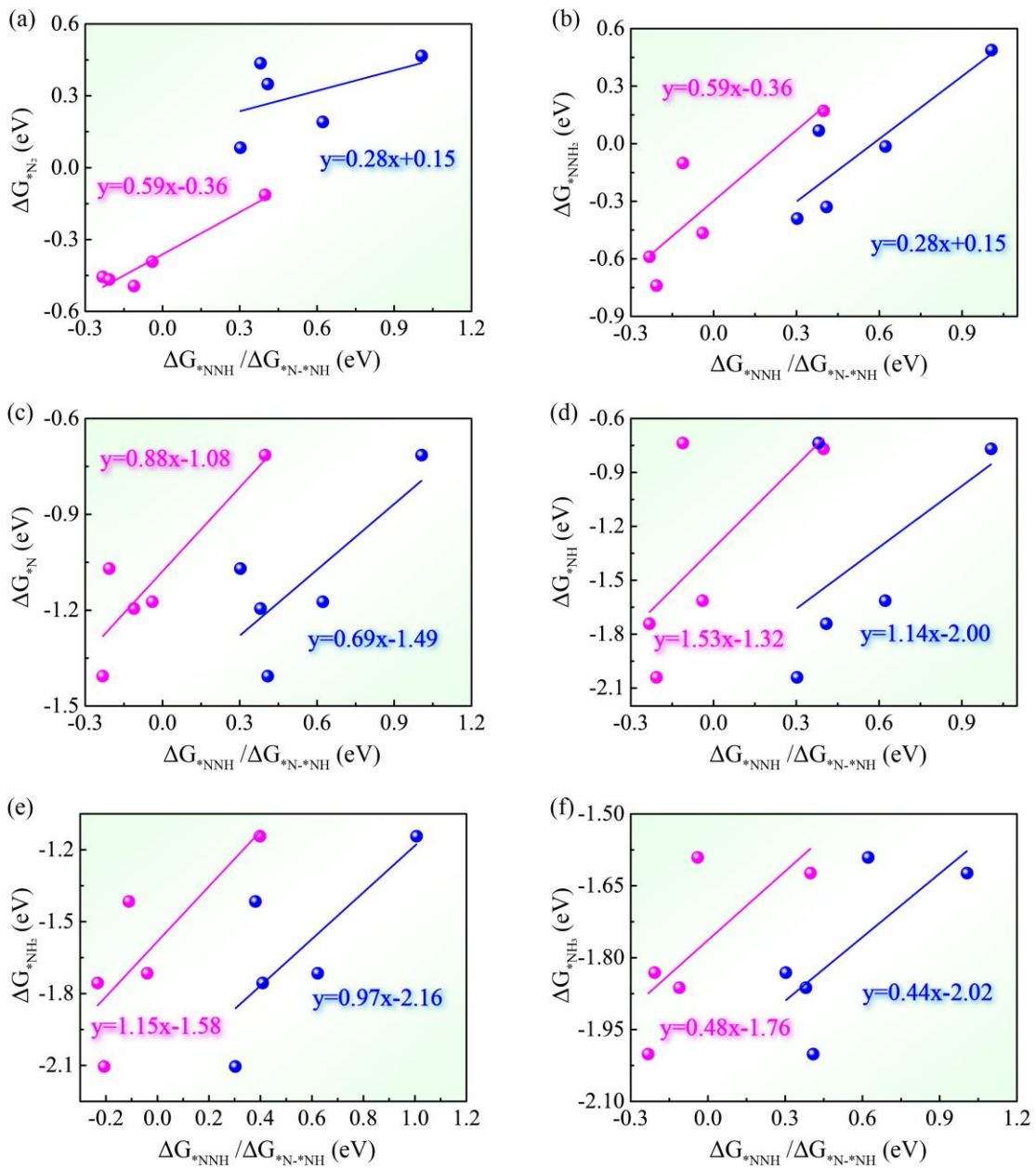


Figure S19. The relationship between the free energy of each NRR elementary step and the Gibbs free energy of *NNH (ΔG_{*NNH}). Rose and blue represent along the distal pathway and along the consecutive pathway, respectively.

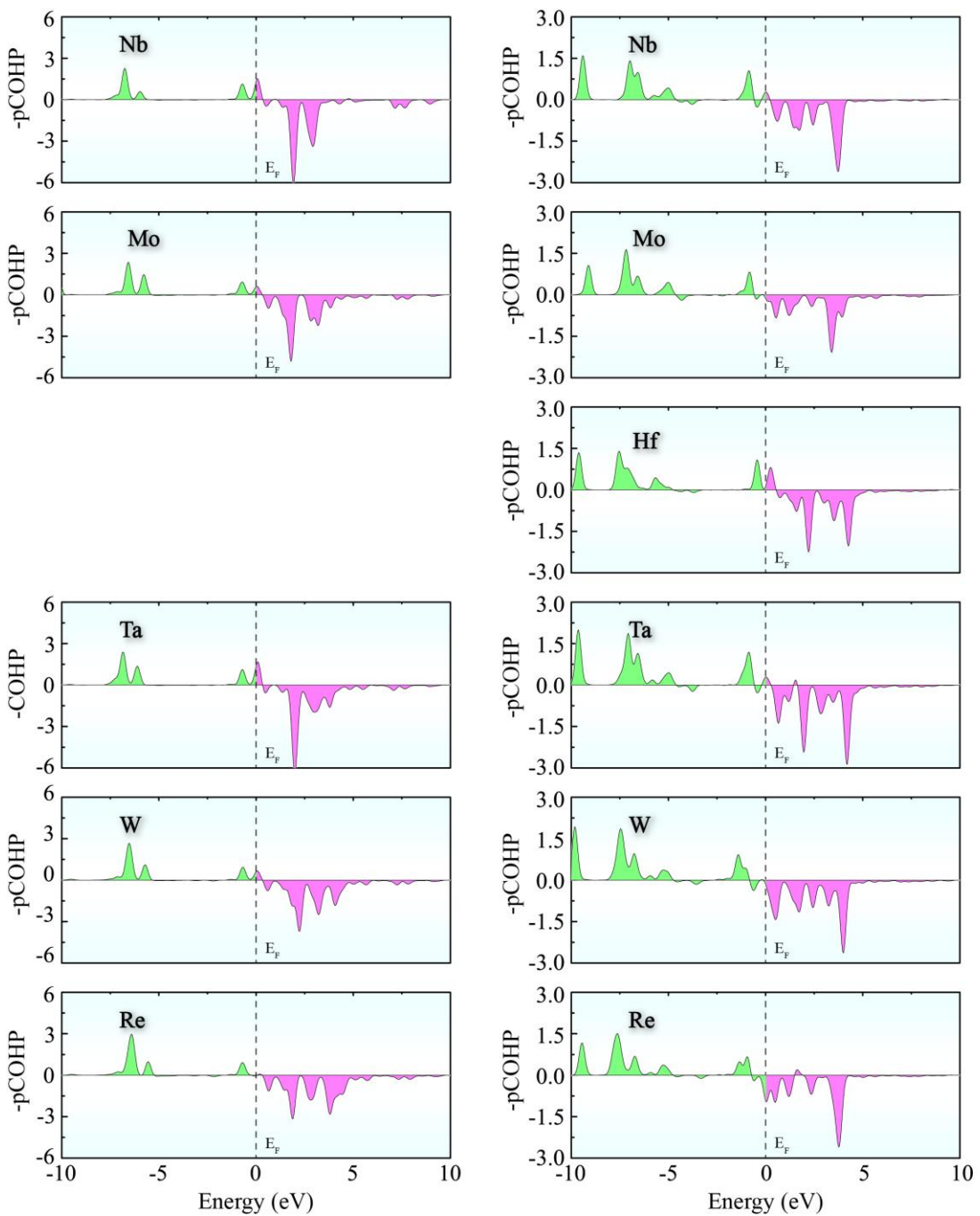


Figure S20. The projected crystal orbital Hamilton population (pCOHP) between TM centers and N_2 intermediate. E_F denotes the Fermi level. The bonding and antibonding contributions are displayed on the left (cyan) and right (rose), respectively.

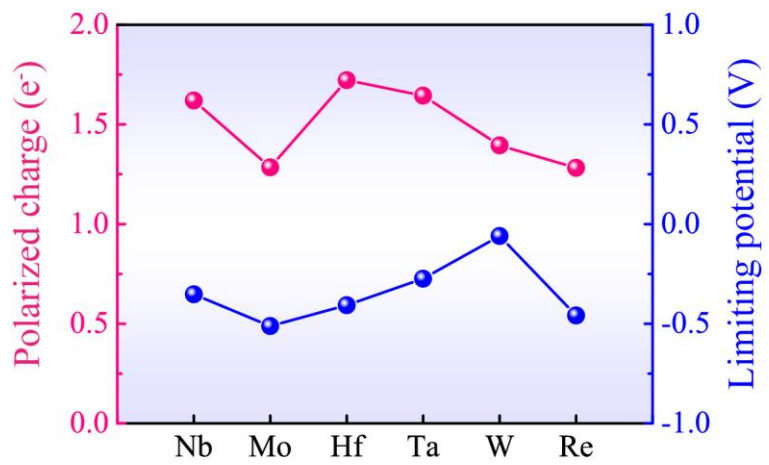


Figure S21. Polarized charge of selected TM@g-C₇N₃ (TM = Nb, Mo, Hf, Ta, W, and Re) catalysts and their corresponding limiting potential of NRR.

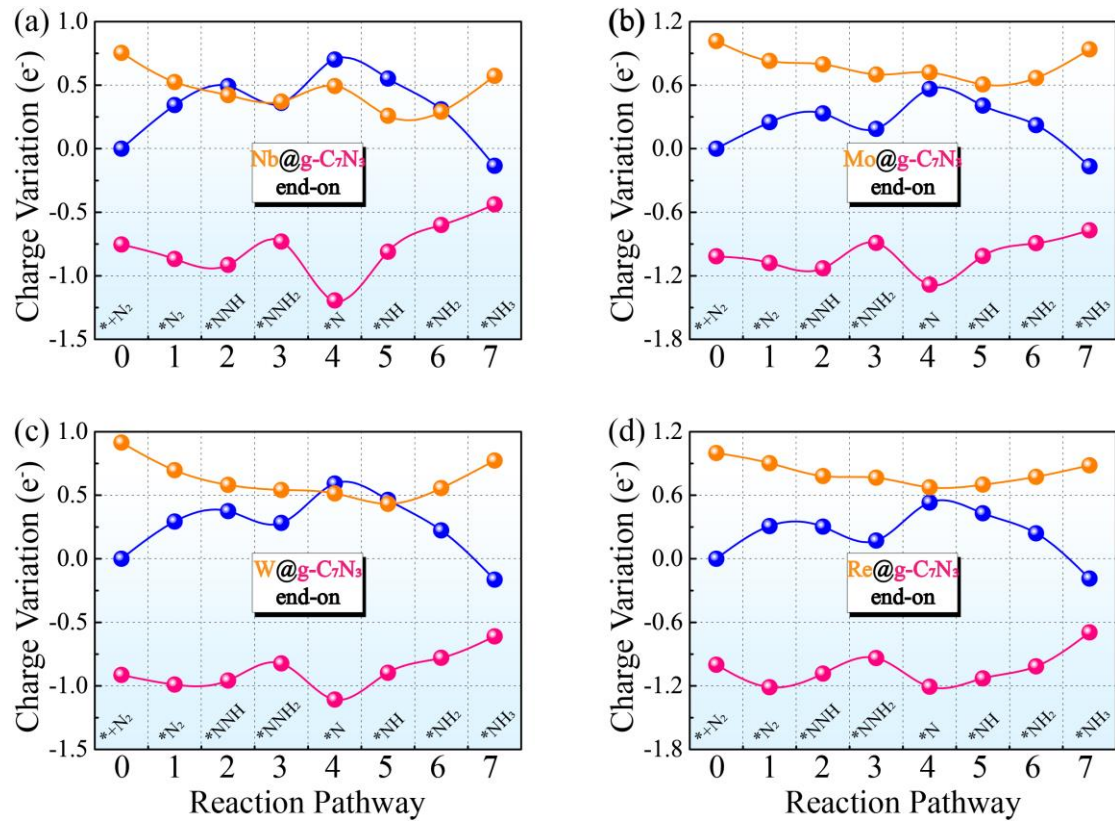


Figure S22. Charge variation of the three moieties for (a) Nb, (b) Mo, (c) W, and (d) Re@g-C₇N₃ via distal pathway, respectively. The definition of moiety is consistent with the Figure 6c.

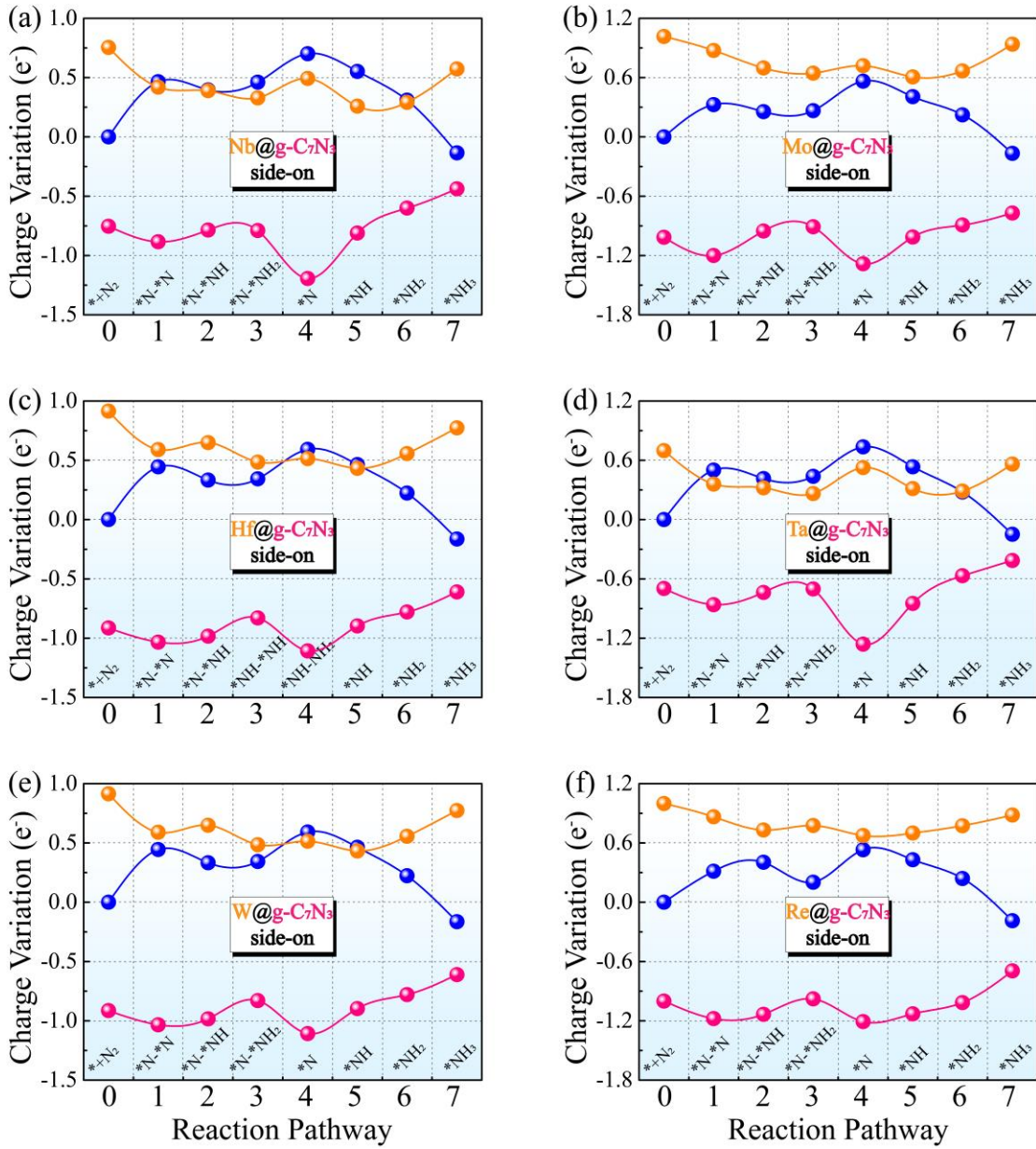


Figure S23. Charge variation of the three moieties for (a) Nb, (b) Mo, (c) Hf, (d) Ta, (e) W, and (e) Re@ $\text{g-C}_7\text{N}_3$. Except that Hf@ $\text{g-C}_7\text{N}_3$ follows mixed pathways, the others follow consecutive pathways. The definition of moiety is consistent with the Figure 6c.

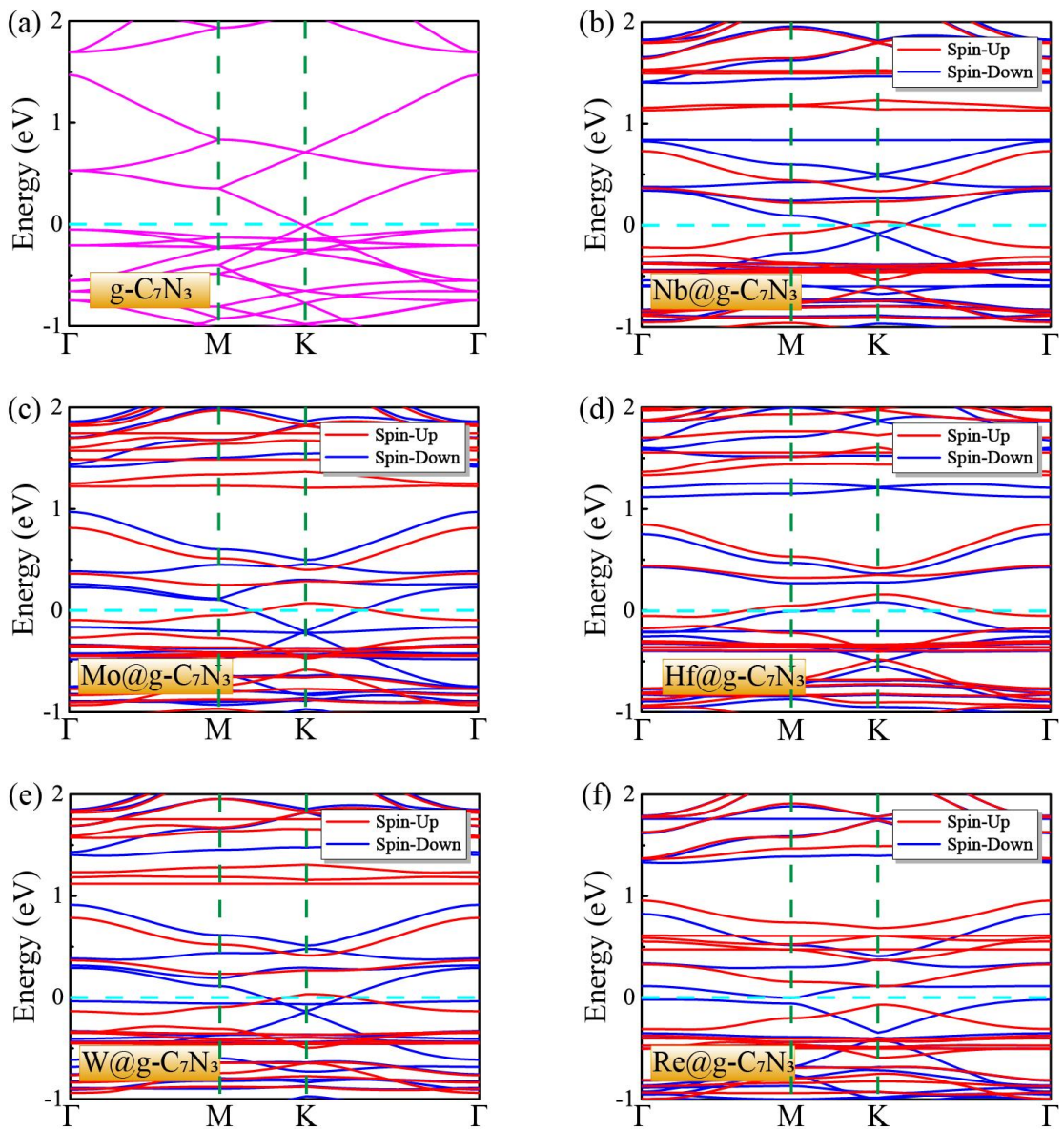


Figure S24. HSE06-predicted band structures of (a) primitive monolayer $g\text{-C}_7\text{N}_3$ and (b) Nb, (c) Mo, (d) Hf, (e) W and (f) $\text{Re}@g\text{-C}_7\text{N}_3$ by HSE06 functional, respectively.

Table S5. Computed vibrational frequencies, zero-point energies, and entropy of reaction intermediates on Nb@g-C₇N₃.

Nb	Vibrational Frequencies (cm ⁻¹)						ZPE (eV)	TΔS (eV)
*N ₂	2072.26	384.05	367.92	342.56	110.70	71.67	0.21	0.14
*NNH	3224.49	1594.44	1158.24	537.00	441.17	378.92	0.49	0.13
	287.17	120.85	108.49					
*NNH ₂	3491.29	3383.69	1614.73	1390.86	1233.32	586.09	0.84	0.14
	561.28	389.19	334.28	326.33	144.98	90.09		
*N	1018.26	230.90	202.86				0.09	0.05
*NH	3486.18	896.69	578.20	532.18	229.52	211.01	0.37	0.07
*NH ₂	3508.60	3405.12	1503.97	685.05	647.76	566.24	0.68	0.10
	333.97	185.93	137.81					
*NH ₃	3499.28	3445.64	3053.27	1614.80	1588.85	1219.69	1.05	0.10
	739.34	692.85	387.98	350.93	176.78	136.84		
*N-*N	1809.50	528.61	329.09	132.70	112.69	103.14	0.19	0.15
*N-*NH	3266.78	1459.34	1181.24	504.39	469.76	338.25	0.47	0.15
	136.52	129.41	115.96					
*N-NH ₂	3472.11	3396.01	1615.09	1144.95	995.70	896.12	0.86	0.12
	723.54	678.61	434.95	173.92	153.85	140.60		
*NHNH	3330.24	3212.58	1479.53	1301.22	1269.32	1008.34	0.82	0.17
	555.06	518.00	253.81	216.18	106.41	54.41		
*NHNH ₂	3472.71	3401.74	3362.19	1618.37	1431.40	1197.42	1.15	0.17
	1135.84	811.55	593.70	557.07	307.31	248.78		
	206.70	113.89	93.35					
*NH ₂ NH ₂	3502.75	3394.13	2856.81	1834.59	1606.72	1418.21	1.35	0.17
	1245.27	1190.79	1026.28	883.13	718.00	503.71		
	461.69	385.56	339.97	303.27	107.57	62.30		
*NH-*NH	3345.76	3295.67	1302.91	1138.33	1012.75	749.68	0.81	0.13
	738.80	499.32	463.66	201.06	169.22	125.18		
*NH-*NH ₂	3503.53	3419.41	3392.15	1613.25	1300.81	1127.55	1.16	0.15
	1072.26	828.43	675.19	618.42	415.39	294.78		
	156.71	135.15	131.29					
*NH ₂ -*NH ₂	3462.87	3448.82	3363.77	3232.04	1601.19	1310.36	1.50	0.14
	1296.82	1144.66	1056.57	918.98	709.13	638.98		
	609.86	440.51	374.69	208.72	169.74	135.96		
*H	1877.30	515.37	503.06				0.18	0.02

Table S6. Computed vibrational frequencies, zero-point energies, and entropy of reaction intermediates on Mo@g-C₇N₃.

Mo	Vibrational Frequencies (cm ⁻¹)						ZPE (eV)	TS (eV)
	2112.97	393.82	366.92	340.35	113.89	67.73		
*N ₂	2112.97	393.82	366.92	340.35	113.89	67.73	0.21	0.14
*NNH	3225.21	1676.66	1115.79	537.75	423.65	393.33	0.49	0.15
	358.54	98.07	67.59					
*NNH ₂	3524.20	3397.79	1605.12	1392.70	1202.19	573.28	0.83	0.15
	445.91	396.04	345.85	311.75	137.68	80.67		
*N	1057.91	205.36	188.63				0.09	0.06
*NH	3386.36	886.08	589.83	564.72	207.31	182.66	0.36	0.07
*NH ₂	3517.56	3402.61	1501.47	724.19	648.60	531.49	0.69	0.09
	387.49	209.25	143.41					
*NH ₃	3490.66	3432.61	2646.20	1614.67	1585.31	1268.61	1.04	0.09
	799.29	733.63	470.94	402.99	199.48	173.51		
*N-*N	1934.92	414.26	231.21	149.55	107.42	85.55	0.18	0.16
*N-*NH	3241.10	1530.33	1152.48	585.17	436.64	378.26	0.48	0.14
	192.62	130.66	107.24					
*N-NH ₂	3472.34	3335.06	1582.05	1127.61	1007.57	826.05	0.84	0.13
	678.51	672.74	439.58	203.66	144.55	104.58		
*NHNH	3246.76	2977.87	1464.42	1434.44	1285.09	1082.40	0.82	0.16
	603.53	448.86	298.92	288.43	106.06	45.10		
*NHNH ₂	3547.63	3436.15	2257.21	1620.44	1466.26	1252.56	1.12	0.17
	1221.58	1004.28	612.86	517.01	395.64	338.90		
	291.28	101.70	38.46					
*NH ₂ NH ₂	3449.51	3425.10	3376.15	2396.99	1640.93	1593.82	1.49	0.17
	1419.19	1302.76	1182.07	1092.01	900.30	762.53		
	443.33	372.55	269.15	231.23	110.51	87.41		
*NH-*NH	3304.28	3239.64	1289.17	1151.31	1026.05	716.66	0.78	0.14
	604.09	471.20	309.61	207.66	145.41	111.21		
*NH-*NH ₂	3486.06	3367.53	2636.35	1611.33	1362.29	1117.82	1.15	0.13
	1054.12	920.71	804.59	765.89	499.24	441.30		
	227.21	162.31	116.20					
*NH ₂ -*NH ₂	3454.09	3430.81	3358.53	3223.33	1585.46	1344.66	1.50	0.13
	1284.74	1120.82	1050.17	925.60	728.67	683.40		
	664.88	468.70	402.06	232.07	176.19	139.12		
*H	1942.45	441.72	335.83				0.17	0.03

Table S7. Computed vibrational frequencies, zero-point energies, and entropy of reaction intermediates on Hf@g-C₇N₃.

Hf	Vibrational Frequencies (cm ⁻¹)						ZPE (eV)	TS (eV)
*N ₂	2124.39	353.89	324.04	314.48	123.64	68.33	0.21	0.14
*NNH	3055.77	1607.91	1243.16	475.09	354.85	308.88	0.46	0.16
	252.81	92.44	73.20					
*N	733.59	133.75	104.48				0.06	0.08
*NH	3554.86	860.43	550.92	541.83	182.90	170.77	0.36	0.08
*NH ₂	3531.05	3434.26	1499.86	661.31	578.90	550.94	0.68	0.11
	369.68	191.72	98.05					
*NH ₃	3469.75	3447.38	3379.25	1625.36	1619.54	1259.24	1.06	0.11
	682.46	669.58	429.70	268.52	154.86	121.43		
*N-*N	1873.73	435.52	315.38	109.40	93.87	35.79	0.18	0.18
*N-*NH	3147.52	1529.21	1293.13	743.93	459.86	432.99	0.50	0.14
	164.74	128.79	108.80					
*N-NH ₂	3430.48	3386.59	1615.75	1150.09	1028.92	855.19	0.84	0.16
	688.93	655.19	400.90	164.91	125.50	45.92		
*NH-*NH	3435.17	3406.29	1308.66	1234.09	1106.42	594.46	0.78	0.17
	473.46	343.79	333.69	170.16	154.99	63.47		
*NH-*NH ₂	3476.52	3463.39	3388.22	1635.60	1263.29	1217.54	1.18	0.14
	1083.28	892.74	739.02	642.61	417.02	352.91		
	193.82	188.61	107.48					
*NH ₂ -*NH ₂	3507.32	3465.69	3421.50	3404.88	1616.61	1593.15	1.53	0.15
	1350.95	1091.35	1073.42	1006.74	905.40	617.02		
	392.55	384.88	342.24	190.66	150.59	129.17		
*H	1806.54	500.58	454.38				0.17	0.02

Table S8. Computed vibrational frequencies, zero-point energies, and entropy of reaction intermediates on Ta@g-C₇N₃.

Ta	Vibrational Frequencies (cm ⁻¹)						ZPE (eV)	TS (eV)
*N ₂	2030.87	407.39	334.77	329.07	130.74	88.54	0.21	0.13
*NNH	3184.44	1594.63	1199.13	551.21	420.02	348.83	0.48	0.14
	317.93	116.41	86.77					
*NNH ₂	3588.03	3472.80	1609.48	1444.00	1189.18	574.33	0.82	0.12
	396.79	369.09	331.49	161.62	128.62	381.67		
*N	995.13	234.27	216.69				0.09	0.05
*NH	3547.10	932.45	603.13	568.64	247.03	221.54	0.38	0.06
*NH ₂	3521.76	3423.85	1504.62	694.00	669.33	548.06	0.68	0.10
	299.80	214.31	146.12					
*NH ₃	3487.76	3436.53	2642.27	1616.24	1576.47	1260.38	1.04	0.09
	802.39	735.65	463.35	414.70	200.51	146.29		
*N-*N	1696.36	585.58	398.26	150.87	111.96	86.73	0.19	0.14
*N-*NH	3309.35	1365.21	1190.30	557.61	487.87	367.15	0.48	0.14
	171.06	145.87	121.73					
*N-NH ₂	3471.30	3397.43	1608.66	1131.76	986.33	902.25	0.86	0.11
	735.74	725.87	445.15	198.28	171.89	162.67		
*NHNH	3306.82	3237.05	1477.22	1317.03	1245.15	946.41	0.82	0.17
	512.82	493.28	297.86	244.96	108.05	30.28		
*NHNH ₂	3457.14	3414.30	3360.18	1621.12	1434.74	1206.52	1.15	0.19
	1136.49	847.80	636.37	551.59	286.09	275.40		
	218.15	85.32	38.26					
*NH ₂ NH ₂	3527.50	3514.21	3421.19	2689.88	1646.73	1640.33	1.40	0.20
	1124.96	1007.37	992.85	957.88	414.70	404.53		
	273.58	248.68	236.92	217.52	138.36	102.61		
*NH-*NH	3376.81	3344.08	1281.38	1121.87	965.51	676.61	0.80	0.12
	633.44	529.78	343.90	234.13	171.30	160.92		
*NH-*NH ₂	3443.52	3434.53	3360.94	1620.19	1286.08	1146.36	1.18	0.14
	1062.92	957.84	773.19	602.41	450.14	352.35		
	190.51	172.21	132.04					
*NH ₂ -*NH ₂	3484.78	3445.09	3351.42	3253.48	1608.05	1290.30	1.50	0.14
	1264.50	1171.03	1066.97	930.67	751.13	640.91		
	609.83	434.69	367.00	213.68	185.31	124.51		
*H	1985.84	533.15	513.57				0.19	4.64

Table S9. Computed vibrational frequencies, zero-point energies, and entropy of reaction intermediates on W@g-C₇N₃.

W	Vibrational Frequencies (cm ⁻¹)						ZPE (eV)	TS (eV)
	2059.66	410.85	375.79	334.83	84.30	64.50		
*N ₂	2059.66	410.85	375.79	334.83	84.30	64.50	0.21	0.15
*NNH	3265.79	1689.63	1105.54	585.62	418.51	401.03	0.49	0.15
	284.39	99.78	63.84					
*NNH ₂	3503.90	3403.38	1612.11	1415.55	1231.41	621.41	0.84	0.14
	567.52	385.19	334.64	323.53	142.17	87.42		
*N	1073.94	232.19	211.96				0.09	0.05
*NH	3476.57	946.36	634.94	602.47	249.07	210.19	0.38	0.06
*NH ₂	3506.07	3402.26	1507.74	720.56	696.83	589.76	0.69	0.10
	370.14	190.95	110.19					
*NH ₃	3484.86	3424.05	2296.06	1602.48	1570.88	1334.99	1.03	0.08
	843.99	793.45	483.95	463.85	224.12	172.38		
*N-*N	1729.28	568.55	390.29	140.29	86.13	121.76	0.18	0.10
*N-*NH	3329.58	1435.29	1154.06	575.02	509.32	401.86	0.49	0.13
	223.09	159.99	122.84					
*N-NH ₂	3475.05	3336.38	1582.98	1116.32	969.02	883.52	0.85	0.12
	743.49	710.52	474.62	207.34	160.62	119.76		
*NHNH	3292.70	3000.11	1522.27	1355.00	1318.94	1093.00	0.84	0.14
	630.30	520.86	273.05	234.79	125.32	108.08		
*NHNH ₂	3469.24	3408.49	3359.16	1611.22	1443.38	1208.81	1.16	0.18
	1152.95	797.06	660.86	577.31	358.21	285.73		
	232.90	76.32	66.88					
*NH ₂ NH ₂	3447.48	3429.39	3374.88	2089.03	1639.62	1590.43	1.48	0.16
	1408.98	1336.94	1189.94	1086.33	892.41	789.11		
	484.07	364.17	304.58	241.80	119.17	99.36		
*NH-*NH	3393.69	3274.39	1268.97	1123.84	980.11	837.44	0.80	0.13
	632.79	517.45	429.28	197.37	156.31	127.96		
*NH-*NH ₂	3475.05	3364.39	2483.05	1588.10	1365.21	1148.92	1.16	0.11
	1052.74	1018.39	846.55	762.36	537.25	485.93		
	241.16	181.17	154.33					
*NH ₂ -*NH ₂	3458.28	3429.65	3316.50	3239.55	1575.70	1312.04	1.51	0.12
	1259.29	1145.82	1046.46	934.55	767.50	696.79		
	650.88	489.66	405.23	233.67	201.55	153.41		
*H	2073.81	526.91	401.25				0.19	0.02

Table S10. Computed vibrational frequencies, zero-point energies, and entropy of reaction intermediates on Re@g-C₇N₃.

Re	Vibrational Frequencies (cm ⁻¹)						ZPE (eV)	TS (eV)
*N ₂	2084.53	507.89	406.57	389.13	96.46	60.93	0.22	0.14
*NNH	3254.58	1714.81	1081.99	577.05	480.62	402.85	0.49	0.04
	337.91	72.71	275.72					
*NNH ₂	3489.43	3341.63	1617.25	1409.43	1235.30	591.96	0.82	0.06
	537.14	453.76	345.63	251.28	62.64	235.53		
*N	1079.02	1079.02	157.85				0.09	0.06
*NH	3446.93	941.78	579.07	307.40	179.40	501.29	0.33	7.64
*NH ₂	3478.97	3428.06	1533.87	846.07	648.03	602.35	0.70	0.11
	438.76	190.42	58.08					
*NH ₃	3458.51	3391.05	2089.00	1608.74	1567.26	1338.56	1.03	0.07
	862.82	830.95	566.15	406.11	260.00	183.28		
*N-*N	1884.10	351.48	192.00	124.37	157.84	268.82	0.16	0.08
*N-*NH	3300.89	1272.54	1122.53	689.63	481.18	418.94	0.47	0.09
	243.95	112.95	164.66					
*N-NH ₂	3394.53	2528.31	1593.90	1154.20	981.19	913.63	0.79	0.05
	808.46	728.07	414.17	231.12	52.84	191.44		
*NHNH	3277.19	2958.77	1502.71	1399.19	1328.31	1082.34	0.82	0.06
	676.88	608.72	272.40	198.87	70.18	256.15		
*NHNH ₂	3477.90	3341.64	3322.83	1616.86	1443.38	1235.11	1.14	0.09
	1140.19	769.25	697.33	632.77	458.28	234.02		
	95.20	138.83	205.81					
*NH ₂ NH ₂	3428.93	3358.26	3306.08	3210.62	1651.33	1569.77	1.50	0.11
	1413.55	1243.94	1126.46	1105.52	875.39	751.62		
	433.72	400.44	143.94	100.31	90.39	212.44		
*NH-*NH	3255.10	3204.10	1352.31	1161.06	971.60	851.11	0.79	0.12
	825.80	458.65	380.33	139.06	79.44	218.12		
*NH-*NH ₂	3389.34	3274.18	2219.37	1619.79	1328.29	1120.34	1.10	0.05
	1075.43	994.60	826.89	783.18	448.10	383.22		
	260.55	94.77	167.91					
*NH ₂ -*NH ₂	3401.86	3354.02	3129.99	3076.96	1599.66	1365.16	1.46	0.07
	1274.97	1145.19	984.05	903.60	821.76	758.24		
	735.97	409.20	356.66	186.74	79.94	252.42		
*H	2159.68	583.08	539.83				0.20	0.01

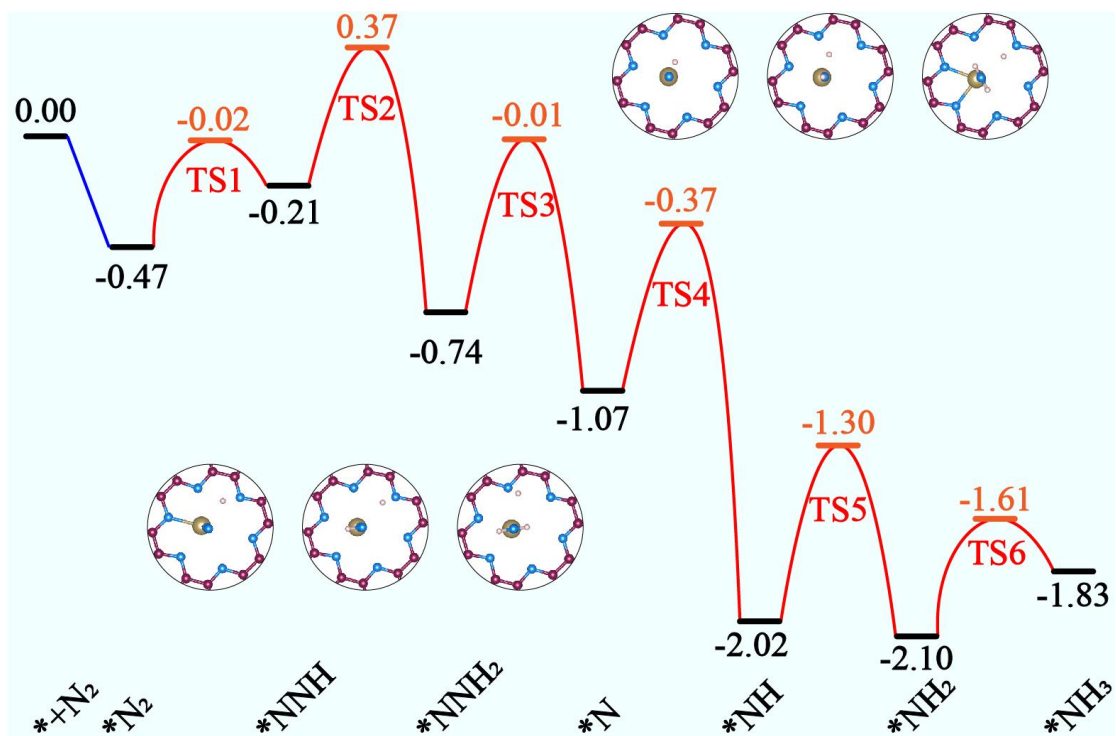


Figure S25. Minimum energy path for N_2 -to- NH_3 . The intermediates and transition states (TS) are marked.

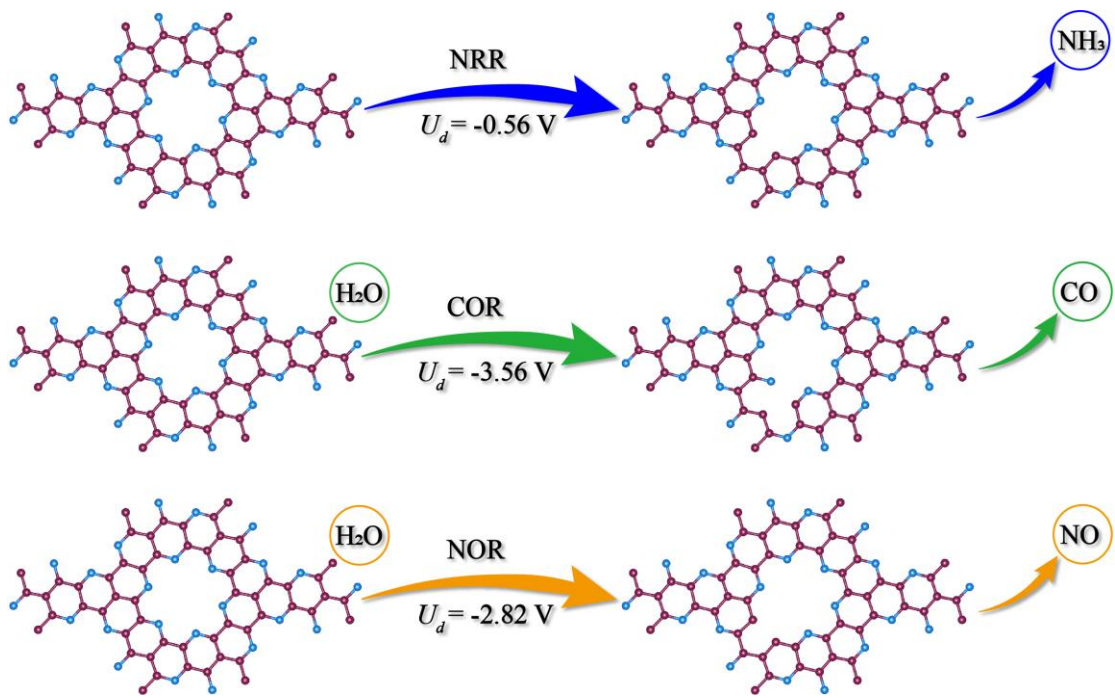


Figure S26. The required potentials of electrochemical decomposition for nitrogen reduction reaction (NRR), carbon oxidation reaction (COR) and nitrogen oxidation reaction (NOR) on $\text{g-C}_7\text{N}_3$.

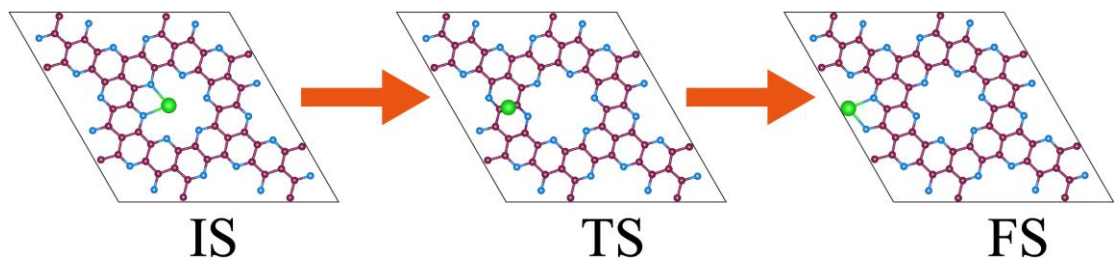


Figure S27. The atomic structures of the initial state (IS), transition state (TS), and final state (FS) during the TM-atom migration from the deposition site to the neighboring site, taking $\text{W}@\text{g-C}_7\text{N}_3$ as an example.

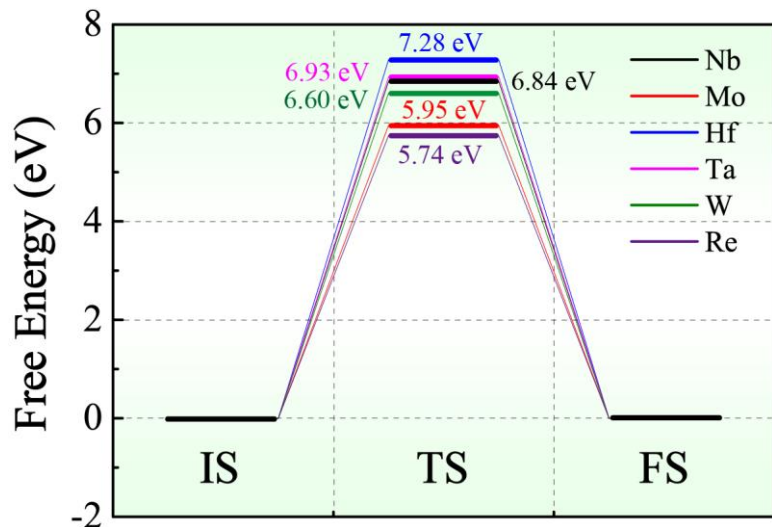


Figure S28. Diffusion energy barriers of Nb, Mo, Hf, Ta, W, Re from the deposition site of g-C₇N₃ to the neighboring site.

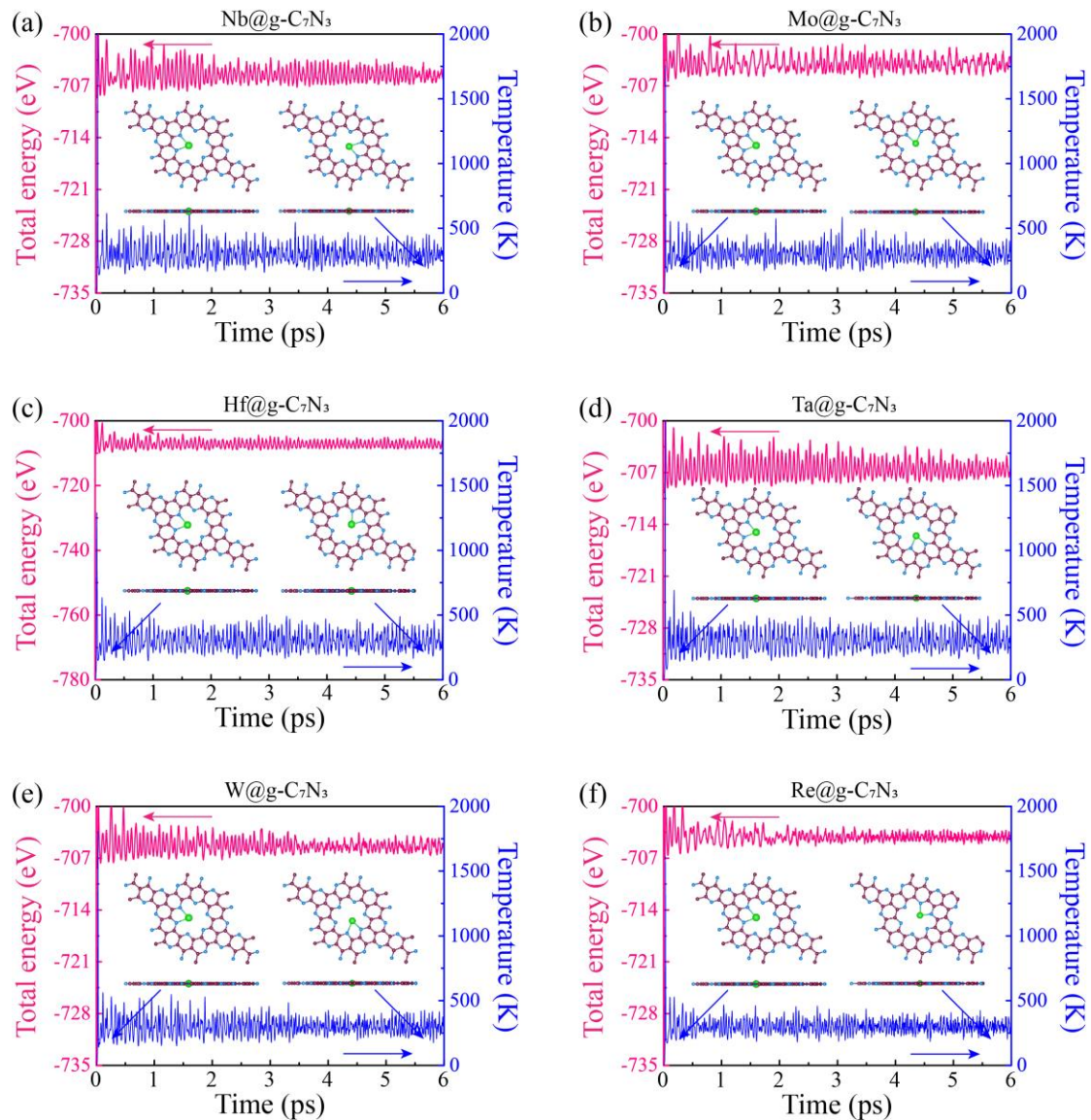


Figure S29. Variations of energy and temperature versus the AIMD simulation time for (a) Nb, (b) Mo, (c) Hf, (d) Ta, (e) W, and (f) Re@g-C₇N₃. The AIMD simulation lasts for 6 ps at 300 K.

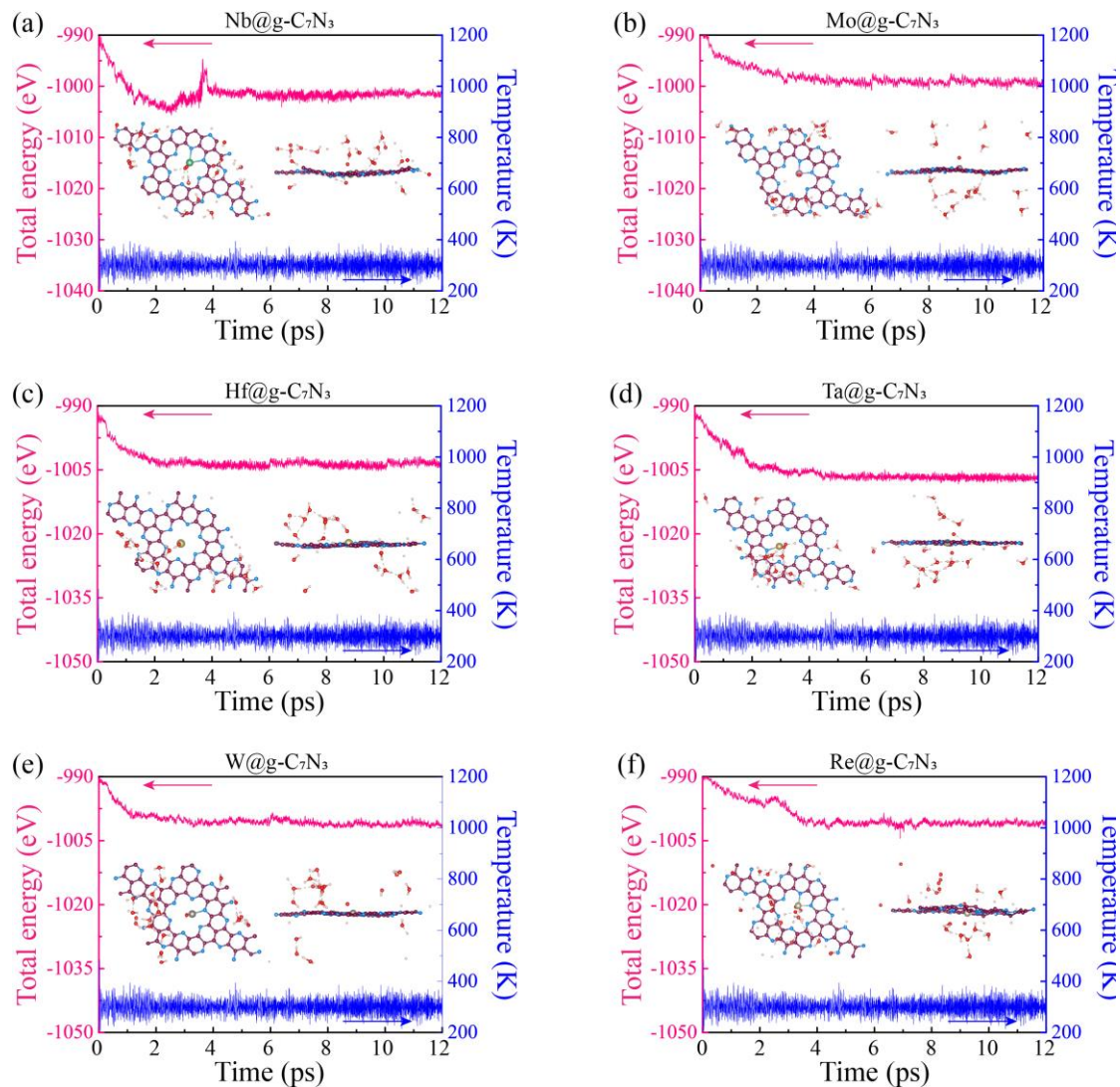


Figure S30. Energy and temperature fluctuations of Nb, Mo, Hf, Ta, W and Re@ $\text{g-C}_7\text{N}_3$ against the time in AIMD simulations at 300 K. To simulate the aqueous solution, the explicit solvent model (about two H_2O layers) is used to simulate the water solution.

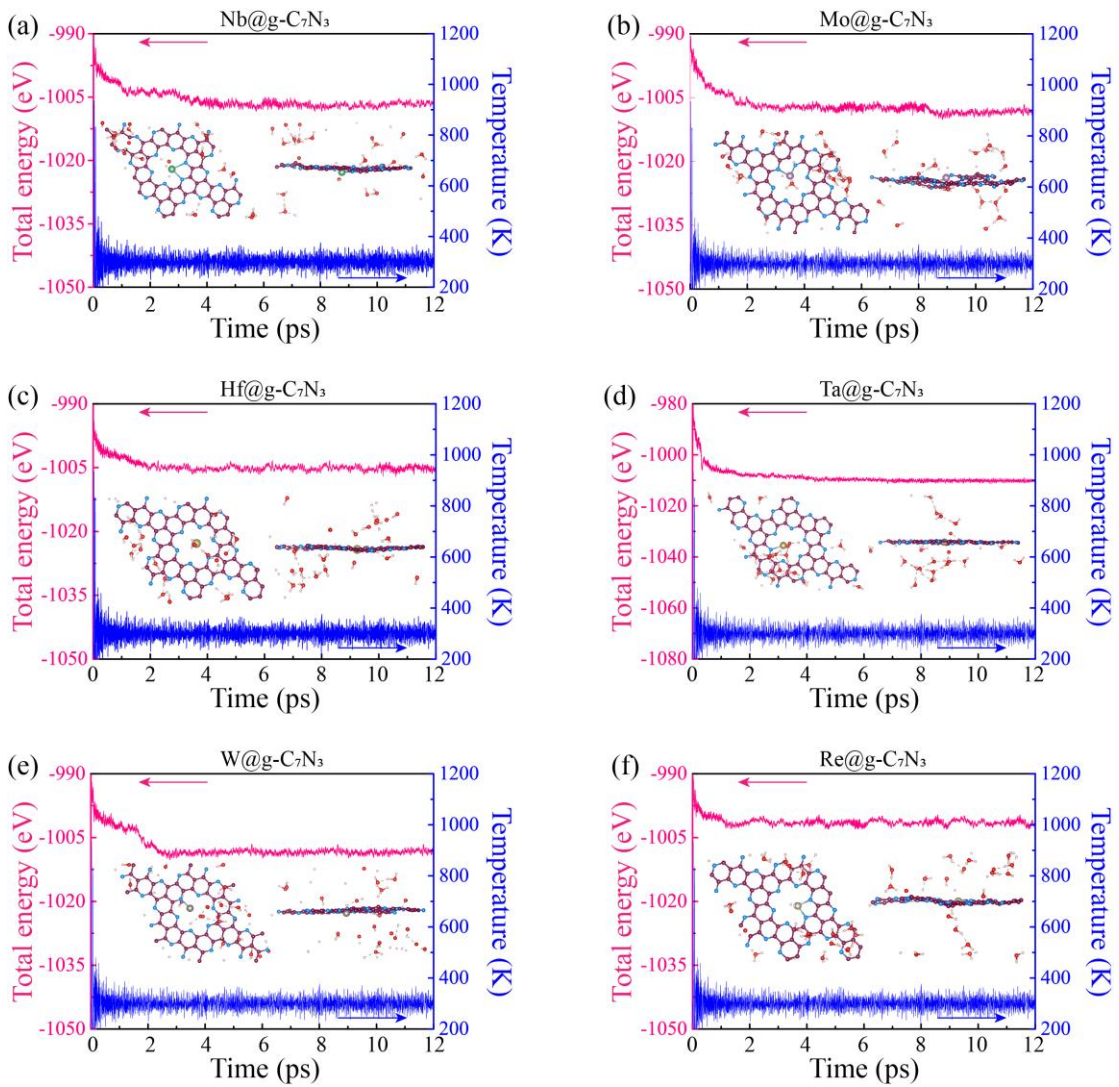


Figure S31. Energy and temperature fluctuations of Nb, Mo, Hf, Ta, W and Re@g-C₇N₃ against the time in AIMD simulations at 300 K. To simulate the acidic aqueous solution, the explicit solvent model (about two H₂O layers) is used and two H atoms are added to simulate the acidic aqueous solution.

Table S11. Formation energy values of Fe/N-G, Co/N-G, Pt/g-C₃N₄, Ru/g-C₃N₄ and TM@g-C₇N₃ (TM = Nb, Mo, Hf, Ta, W and Re).

Catalyst	E _f (eV)	Ref.
Nb@g-C ₇ N ₃	-0.93	this work
Mo@g-C ₇ N ₃	-0.51	this work
Hf@g-C ₇ N ₃	-3.79	this work
Ta@g-C ₇ N ₃	-1.56	this work
W@g-C ₇ N ₃	0.72	this work
Re@g-C ₇ N ₃	1.45	this work
Fe/N-G	2.26	⁷
Co/N-G ₅	2.27	⁸
Pt/g-C ₃ N ₄	2.88	⁹
Ru/g-C ₃ N ₄	3.12	¹⁰

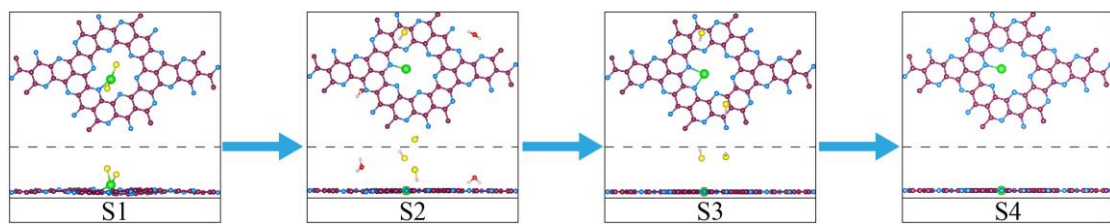


Figure S32. The designed synthetic route for TM@g-C₇N₃. Yellow and red atoms represent Cl and O atoms, respectively.

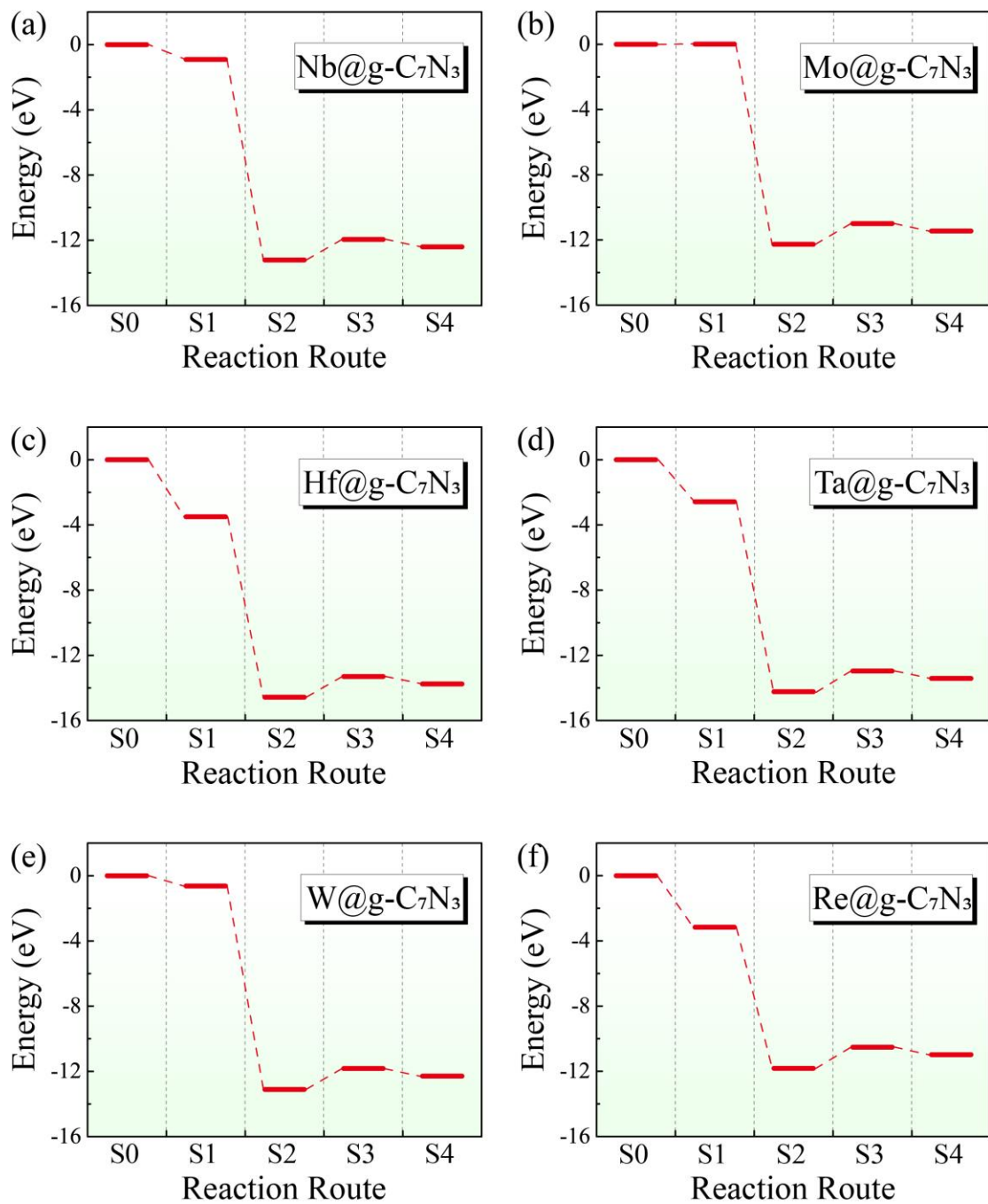


Figure S33. The energy profiles of the synthetic route including (a) Nb@ g-C₇N₃, (b) Mo@ g-C₇N₃, (c) Hf@ g-C₇N₃, (d) Ta@ g-C₇N₃, (e) W@ g-C₇N₃, and (f) Re@g-C₇N₃, where S0 represents the primitive g-C₇N₃ monolayer.

References

- 1 J.K. Nørskov, T. Bligaard, A. Logadottir, J.R. Kitchin, J.G. Chen, S. Pandelov, U. Stimming, *J. Electrochem. Soc.*, 2005, **152**, J23-J26.
- 2 A.A. Peterson, F. Abild-Pedersen, F. Studt, J. Rossmeisl, J.K. Nørskov, *Energy Environ. Sci.*, 2010, **3**, 1311-1315.
- 3 W. Zhao, L. Zhang, Q. Luo, Z. Hu, W. Zhang, S. Smith, J. Yang, *ACS Catal.*, 2019, **9**, 3419-3425.
- 4 X. Liu, Y. Jiao, Y. Zheng, M. Jaroniec, S.-Z. Qiao, *J. Am. Chem. Soc.*, 2019, **141**, 9664-9672.
- 5 X. Lv, W. Wei, H. Wang, B. Huang, Y. Dai, *Appl. Catal. B*, 2020, **264**, 118521.
- 6 J. Wu, J.H. Li, Y.X. Yu, *ACS Appl. Mater. Interfaces*, 2021, **13**, 10026-10036.
- 7 D. Deng, X. Chen, L. Yu, X. Wu, Q. Liu, Y. Liu, H. Yang, H. Tian, Y. Hu, P. Du, R. Si, J. Wang, X. Cui, H. Li, J. Xiao, T. Xu, J. Deng, F. Yang, P.N. Duchesne, P. Zhang, J. Zhou, L. Sun, J. Li, X. Pan, X. Bao, *Sci. Adv.*, 2015, **1**, e1500462.
- 8 H. Fei, J. Dong, M.J. Arellano-Jiménez, G. Ye, N. Dong Kim, E.L.G. Samuel, Z. Peng, Z. Zhu, F. Qin, J. Bao, M.J. Yacaman, P.M. Ajayan, D. Chen, J.M. Tour, *Nat. Commun.*, 2015, **6**, 8668.
- 9 X. Li, W. Bi, L. Zhang, S. Tao, W. Chu, Q. Zhang, Y. Luo, C. Wu, Y. Xie, *Adv. Mater.*, 2016, **28**, 2427-2431.
- 10 S. Tian, Z. Wang, W. Gong, W. Chen, Q. Feng, Q. Xu, C. Chen, C. Chen, Q. Peng, L. Gu, H. Zhao, P. Hu, D. Wang, Y. Li, *J. Am. Chem. Soc.*, 2018, **140**, 11161-11164.